Stony Brook University

Design of ultra-sensitive fluorescence detection system for applications in molecular biology.

A Dissertation Presented

by

Ivan Tovkach

to

The Graduate School

in Partial Fulfillment of the

Requirements

for the Degree of

Doctor of Philosophy

in

Electrical Engineering

Stony Brook University

December 2013

Stony Brook University

The Graduate School

Ivan Tovkach

We, the dissertation committee for the above candidate for the

Doctor of Philosophy degree, hereby recommend

acceptance of this dissertation.

Vera Gorfinkel – Dissertation Advisor

Associate Professor, Department of Electrical and Computer Engineering

Dmitri Donetski - Chairperson of Defense

Assistant Professor, Department of Electrical and Computer Engineering

Leon Shterengas

Assistant Professor, Department of Electrical and Computer Engineering

Dmitriy Beznosko

Assistant Professor, Department of Physics, Nazarbayev University

This dissertation is accepted by the Graduate School

Charles Taber
Dean of the Graduate School

Abstract of the Dissertation

Design of ultra-sensitive fluorescence detection system for applications in molecular biology.

by

Ivan Tovkach

Doctor of Philosophy

in

Electrical Engineering

Stony Brook University

2013

I present a new universal data acquisition system for application for fluorescence detection in life sciences. The system is based on fiberized spectrometer bench with multichannel single photon sensor. Two different spectrometers were designed and tested. One is based on 32 channels PMT and another based on fiberized array of 48 avalanche photo diodes. The developed detection system was tested for three different applications including: DNA sequencing, detection of color encoded beads and fluorescence activated bead sorting.

The system is capable of detecting multicolor fluorescence produced by mixtures of fluorescent dyes as well as by micro and nano-objects. In the system, the analyzed sample is forced into the capillary by applying either air pressure or electric field. When the sample passes through a detection area, a laser beam induces multi-color fluorescence. Polychromatic fluorescence is collected by a fiber and directed to the single photon spectrometer. The spectrometer performs color separation and the measurement of fluorescence in the range of wavelengths from 480nm to 720nm. The fluorescence which comes to the spectrometer through the input fiber is coupled to a collimator which produces a parallel polychromatic beam of 10mm diameter. The parallel beam passes through laser rejection filters and undergoes separation on the diffraction grating into constituent wavelength components. The decomposed polychromatic light is received by a multi-channel single photon sensor. The obtained photon count is transferred to computer for recording and data processing. The unique combination of

fluorescent dyes with known spectra is recognized in each individual measurement by using color deconvolution of the dye's spectra.

The developed fluorescence detection system can be used in wide variety of devices for molecular diagnostics and medicine.

Table of Contents

List of Figures

List of Abbreviations

Abbreviation or Symbol	Term
APD	Avalanche Photodiode
CE	Capillary Electrophoresis
DC	Dark Counts
OD	Optical Density
LIF	Laser Induced Fluorescence
PCB	Printed Circuit Board
PCR	Polymerase Chain Reaction
PMT	Photomultiplier Tube
SiPM	Silicon Photomultiplier
SPAD	Single Photon Avalanche Diode

I. INTRODUCTION

One of very important practical tasks in molecular biology is creation of multiplex measurements, when multiple biological reporters can be processed and measured within one experiment. In order to introduce multiplexing, it is common to use mutli-color fluorescent markers for biological molecules. Another very efficient method for multiplex measurements is the use of color-encoded micro-beads. In this case the color encoding can be introduced due to the use of various compositions of several fluorescence dyes. For example, company Luminex offers up to 500 various types of encoded beads which are colored with only three colors. Recently a number of technologies have been developed for optical "bar coding" of micro- and nano-objects (beads, cells, etc.) using multi-color fluorescence. This includes the use of segmented nanorods [Nicewarner-Pena, S. R, 2001], rare-earth doped glass [Dejneka, M. J, 2003], fluorescent silica colloids [Grondahl, L, 2000], photobleached patterns [Braeckmans, K., 2003], enhanced Raman nanoparticles [Mulvaney, S. P., 2003] and semiconductor quantum dots (QD) [Gao, X.; Nie, S., 2003, 2004].

The goal of my work is design and development of a novel data acquisition system which allows a highly sensitive, accurate and fast detection of multicolor, laser induced fluorescence (LIF). The applications of our system will be in measurements and characterization of various biological molecules carried in solutions by different means (electrophoresis, fluidic pumping, molecules carried on micro-beads, etc.). Biological applications of our system will be detection and quantification of bio-molecules (proteins, RNA, DNA), which is very important in molecular biology and medicine.

The main goal of my work

My main goal was to design and develop a system which would be able to detect thousands of color combinations due to the use of single photon spectrometer in conjunction with appropriate fluidic system and software.

Detailed description of the system modules is presented in Chapters 1-2, and in Chapter 3 describes applications of the developed system for measurement of composition of fluorescent dyes and measurements of beads encoded with fluorescent dyes and quantum dots.

Operation of the system

The system consists of two main modules: single photon spectrometer and capillary sample analyzer, and an external laser source (in my work I used various commercial lasers which were fiberized with either single-mode or multi-mode fibers). The architecture of the system is such that the modules are connected via optical fibers and the detected signals are transferred to computer for recording and processing (see Figure 1. Architecture of the system). In the system a fiberized laser source delivers excitation power to a capillary sample analyzer. In the analyzer, fluorescent objects are moved through the capillary in which they are illuminated by the laser, their fluorescence is collected by a fiberized optical collection system and delivered to a fiberized spectrometer. In the spectrometer, after color decomposition the fluorescent signal is detected by a multi-channel single photon detector, the detected signals are transferred to the computer.

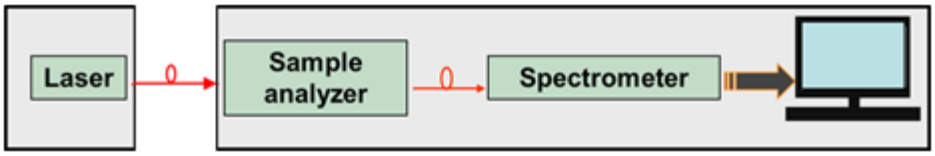

Figure 1. Architecture of the system

Approach to system design

Our approach to system design is presented in Figure 2. Approach to system design and development.

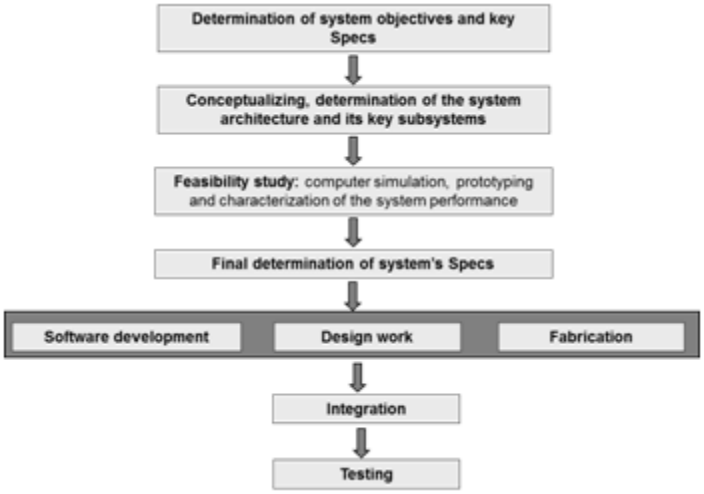

Figure 2. Approach to system design and development.

CHAPTER 1. SPECTROMETR

1.1.System objectives and key specs

Our system is intended for highly sensitive, accurate and fast detection and recognition of fluorescence encoded micro- and nano-objects. Since our system is intended to detect very weak fluorescent signals, we select single photon counting as a detection method.

In order to have a high detection throughput, we need to be able to detect up to 10,000 events per second (~20mks/event). In order to ensure high detection accuracy, our spectrometer must have broad linearity range and high frame rate.

The target specs for the spectrometer are presented below:

Spectral range	520-750nm (*determined by fluorescent dyes used*)
Spectral resolution	5-10nm/channel (*based on spectral width of fluorescent dyes ~50nm*)
Linearity:	10^8/s per channel
Frame rate:	1MHz
Data recording rate:	32MB/s via USB port

Operation of the spectrometer

Block-diagram of single photon spectrometer is presented in Figure 3. Schematic of spectrometer.

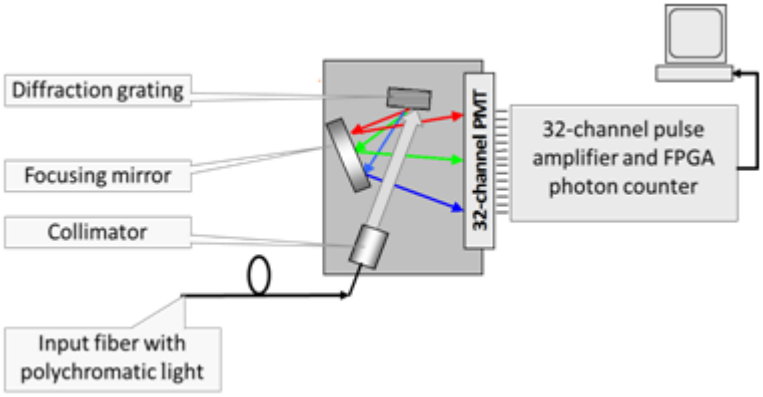

Figure 3. Schematic of spectrometer.

In the spectrometer polychromatic light delivered through optical fiber, passes through collimator, gets decomposed by a diffraction grating, and focused onto photocathodes of 32-channel PMT. The signals detected by the PMT are amplified by high frequency pulse amplifier, counted by FPGA photon counter and transferred to computer.

1.2.Theoretical background

Calculations

Diffraction grating

The diffraction grating is of considerable importance in spectroscopy, due to its ability to separate (disperse) polychromatic light into its constituent monochromatic components. In recent years, the spectroscopic quality of diffraction gratings has greatly improved, and Newport has been a leader in this development.

The extremely high accuracy required of a modern diffraction grating dictates that the mechanical dimensions of diamond tools, ruling engines, and optical recording hardware, as well as their environmental conditions, be controlled to the very limit of that which is physically

possible. A lower degree of accuracy results in gratings that are ornamental but have little technical or scientific value. The challenge to produce precision diffraction gratings has attracted the attention of some of the world's most capable scientists and technicians. Only a few have met with any appreciable degree of success, each limited by the technology available.

A *diffraction grating* is a collection of reflecting (or transmitting) elements separated by a distance comparable to the wavelength of light under study. It may be thought of as a collection of diffracting elements, such as a pattern of transparent slits (or apertures) in an opaque screen, or a collection of reflecting grooves on a substrate (also called a *blank*). In either case, the fundamental physical characteristic of a diffraction grating is the spatial modulation of the refractive index. Upon diffraction, an electromagnetic wave incident on a grating will have its electric field amplitude, or phase, or both, modified in a predictable manner, due to the periodic variation in refractive index in the region near the surface of the grating.

A *reflection grating* consists of a grating superimposed on a reflective surface, whereas a *transmission grating* consists of a grating superimposed on a transparent surface.

A *master grating* (also called an *original*) is a grating whose surface-relief pattern is created “from scratch”, either by mechanical ruling or holographic recording. A *replica grating* is one whose surface relief pattern is generated by casting or molding the relief pattern of another grating.

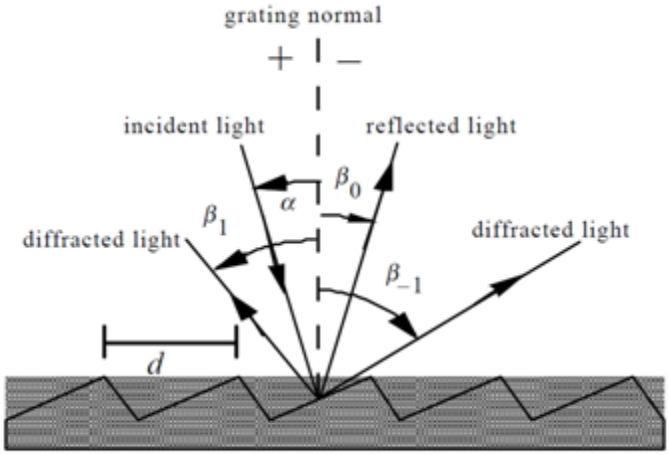

Figure 4. Diffraction grating ray geometry.

When a grating depends on the fact that there exists a unique set of discrete angles along which, for a given spacing *d* between grooves, the diffracted light from each facet is in phase with the light diffracted from any other facet, leading to constructive interference.

Diffraction by a grating can be visualized from the geometry in Figure 4. Diffraction grating ray geometry. which shows a light ray of wavelength *l* incident at an angle *a* and diffracted by a grating (of *groove spacing d*, also called the *pitch*) along at set of angles {*bm*}. These angles are measured from the grating normal, which is shown as the dashed line perpendicular to the grating surface at its center. The sign convention for these angles depends on whether the light is diffracted on the same side or the opposite side of the grating as the incident light. In Figure 1.2.1 which shows a *reflection grating*, the angles $a > 0$ and $b1 > 0$ (since they are measured counter-clockwise from the grating normal) while the angles $b0 < 0$ and $b{-}1 < 0$ (since they are measured clockwise from the grating normal)

Spectrometer calculations

Schematic of the optical system of the spectrometer is shown in Figure 5. Schematic and measurements of the spectrometer.

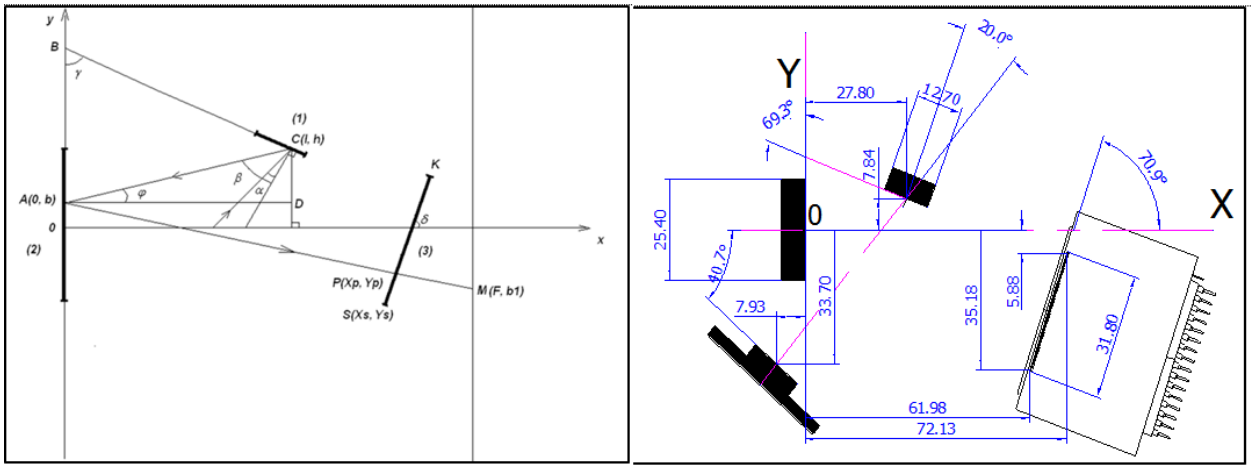

Figure 5. Schematic and measurements of the spectrometer.

Polychromatic light impinged on the grating (1) has incident angle α, reflected on mirror (2) has angle β, reflected one more time on detector and has angle F.

Positions and dimensions of diffraction grating, mirror and detector are given in Figure 5. Schematic and measurements of the spectrometer.(left panel).

Now we need to find which channel of the detector is illuminated by the back light ray.

1. Let's find correlation between angles α, β, φ .

We know equation for angles correlation between incident light and reflected light on diffraction grating

$$\beta = \arcsin\left(\frac{m\lambda}{d_{DG}} - \sin\alpha\right), \qquad (1)$$

Where

$m = 0, \pm 1, \pm 2 \ldots$,

α- wavelength

d_{DG} - parameters of diffraction grating.

From the drawing we can see that:

$$\varphi + \beta + \frac{\pi}{2} + \pi - \gamma = \pi$$

Therefore,

$$\varphi = \gamma - \beta - \frac{\pi}{2}.$$

From triangle ΔACD we can find ***b***:

$tg\varphi = \frac{h-b}{l}$, from her we can find next equation

$$b_\beta = h - l \cdot tg\varphi. \qquad (2)$$

We know that $-tg\varphi = \frac{b_1}{F}$, then

$$b_1 = -F \cdot tg\varphi. \qquad (3)$$

2. Let's find point where incident light beam crosses axle OY.

Angle between incident ray and positive direction OX, equal $\gamma - \frac{\pi}{2} - \alpha$, and crosses point $C(l,h)$ on grating. Then equation of incident ray will be:

$$y = -x \cdot ctg(\gamma - \alpha) + h + l \cdot ctg(\gamma - \alpha).$$

Let's call coordinate point where incident light ray and axe OY as point b_α.

Then we have

$$b_\alpha = h + l \cdot ctg(\gamma - \alpha)$$

3. Now we'll find cross point reflected light ray from mirror and detector

This ray crosses two point that we know A(0, b) and $M(F, b_1)$.

From here we have:

$$y = \frac{b_1 - b}{F} x + b.$$

Detector is on the line that creates angle δ, with axe OX and crosses point $S(x_s, y_s)$.

Then equation for the line that crosses detector:

$$y = x \cdot tg\delta + Y_s - X_s \cdot tg\delta.$$

Now we need to find cross point between these two lines. To do that we need to solve equation:

$$\begin{cases} y = \dfrac{b_1 - b}{F} x + b \\ y = x \cdot tg\delta + Y_s - X_s \cdot tg\delta \end{cases}$$

Solution is:

$$X_{PMT} = \frac{X_s \cdot tg\delta - Y_s + b}{F \cdot tg\delta - b_1 + b} \cdot F \qquad (4)$$

$$Y_{PMT} = \frac{(b_1 - b) \cdot \left(X_s \cdot tg\delta - Y_s + b \right)}{F \cdot tg\delta - b_1 + b} + b$$

.

Now we find $PS = \sqrt{(X_s - X_{PMT})^2 + (Y_s - Y_{PMT})^2}$ (5).

Point K belongs to the first channel and point S - to the channel number 32.

Then point P belongs $\dfrac{32\left(q - PS\right)}{q}$ channel, where q - detector length. (6)

4. Now we need to find cross point of the reflected ray from the mirror, and diffraction grading.

Diffraction grating is located on a line that has creates angle γ with axe OX, and crosses though the middle of diffraction grading that has coordinates (l_0, h_0)

Now we can find equation for the line that crosses diffraction grading:

$$y = x \cdot tg\gamma + h_0 - l_0 \cdot tg\gamma \,.$$

In order to find cross point between these two lines we need to solve these equations:

$$\begin{cases} y = \dfrac{b_1 - b}{F} x + b \\ y = x \cdot tg\gamma + h_0 - l_0 \cdot tg\gamma \end{cases}$$

Solution is:

$$x_{DG} = \frac{l_0 \cdot tg\gamma + h_0 - b}{F \cdot tg\gamma + b_1 - b} \cdot F \qquad (7)$$

$$y_{DG} = \frac{(b_1 - b)\left(l_0 \cdot tg\gamma + h_0 - b\right)}{F \cdot tg\gamma + b_1 - b} + b \,.$$

These points should satisfy next:

$$\begin{cases} l_{\min} \le X_{DG} \le l_{\max} \\ h_{\min} \le Y_{DG} \le h_{\max} \end{cases} \qquad (8)\,,$$

Where $l_{\min}, h_{\min}, l_{\max}, h_{\max}$ determined as.

$$C_{max}: \begin{cases} l_{\max} = l_0 - \left(-\frac{D}{2}\cos\gamma \right) = l_0 + \frac{D}{2}\cos\gamma \\ h_{\max} = h_0 + \frac{D}{2}\sin\gamma = l_0 + \frac{D}{2}\sin\gamma \end{cases} \quad (9)$$

$$C_{\min}: \begin{cases} l_{\min} = l_0 + \left(-\frac{D}{2}\cos\gamma \right) = l_0 - \frac{D}{2}\cos\gamma \\ h_{\min} = h_0 - \frac{D}{2}\sin\gamma = l_0 - \frac{D}{2}\sin\gamma \end{cases}$$

If reflected ray crosses diffraction grating, then we can use next equations:

$$\begin{cases} x_{DG} = l_{\min} \\ \frac{b-b_1}{F} l_{\min} + b - h_{\min} \geq 0 \end{cases} \quad \text{and} \quad \begin{cases} x_{DG} = l_{\max} \\ \frac{b-b_1}{F} l_{\max} + b - h_{\max} \leq 0 \end{cases} \quad (10)$$

5. Now let's say we have the light ray, with specific wavelength, that crosses point $C_{\min}$ with angle α, and angle $\varphi = 0$.

Now we need to determine angle α that satisfies $\varphi = 0$.

We know

$$\varphi = \gamma - \beta - \frac{\pi}{2},$$

than $0 = \gamma - \beta - \frac{\pi}{2} \Rightarrow \beta = \gamma - \frac{\pi}{2}$.

Therefore,

$$\beta_{\varphi=0} = \gamma - \frac{\pi}{2} = \arcsin\left(\frac{m\lambda}{d_{DG}} - \sin\alpha_{\varphi=0}\right), \quad \left|\frac{m\lambda}{d_{DG}} - \sin\alpha_{\varphi=0}\right| \le 1.$$

We need to solve this equation:

$$\sin\left(\gamma - \frac{\pi}{2}\right) = \sin\left(\arcsin\left(\frac{m\lambda}{d_{DG}} - \sin\alpha_{\varphi=0}\right)\right)$$

$$-\cos\gamma = \frac{m\lambda}{d_{DG}} - \sin\alpha_{\varphi=0}$$

$$\sin\alpha_{\varphi=0} = \frac{m\lambda}{d_{DG}} + \cos\gamma$$

$$\alpha_{\varphi=0} = \arcsin\left(\frac{m\lambda}{d_{DG}} + \cos\gamma\right), \quad \left|\frac{m\lambda}{d_{DG}} + \cos\gamma\right| \le 1 \qquad (11)$$

If we'll increase angle α, then some specific ray with specific wavelength will cross diffraction grating. For each wavelength we'll have different angle $\alpha_{\varphi=0}$. To avoid situation when

reflected ray crosses diffraction grating, incident light ray should have angle that satisfy:

$< \min\left\{\alpha_{\varphi=0,\lambda_1}, \alpha_{\varphi=0,\lambda_2}, \alpha_{\varphi=0,\lambda_3}, ...\right\}$.

1.3.Design of 32-channel spectrometer

Based on the obtained equations we carried out preliminary calculations of the spectrometer.

Final calculations were carried our using CAD package (Figure 6. Ray tracing in spectrometer)

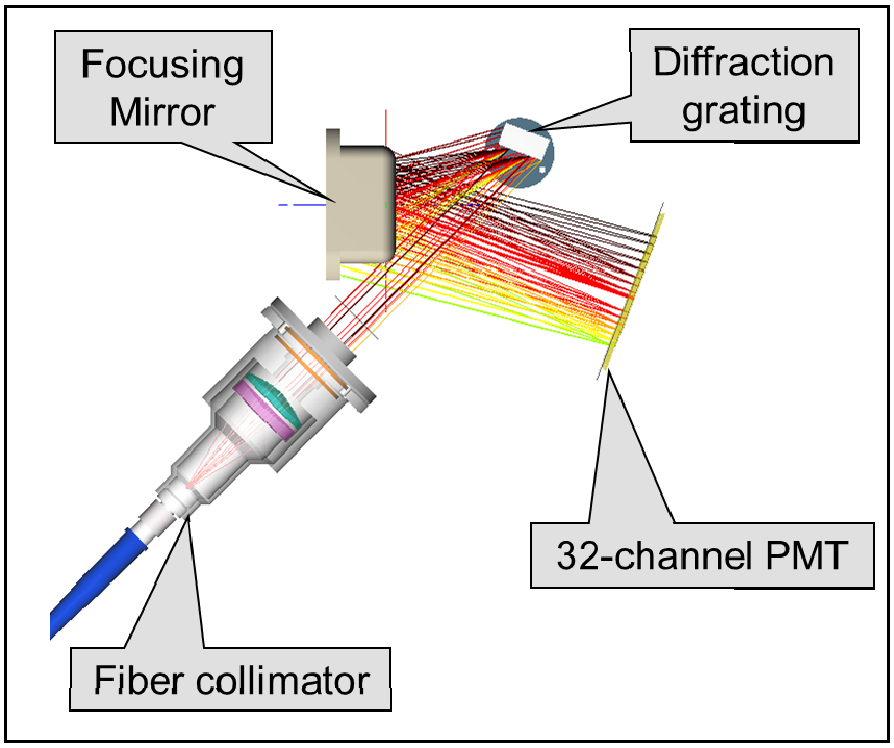

Figure 6. Ray tracing in spectrometer

The spectrometer was designed based on the following commercial components:

1. The SMA Optical fiber core diameter 200mkm
2. The F810SMA Series of fiber collimation
3. Thorlabs GR13-1850 - ruled diffraction grating, 1800/mm, 500 nm Blaze, 12.7 x 12.7 x 6 mm
4. CM254-050-G01 - Ø1" Aluminum-Coated Concave Mirror, f=50 mm
5. Filters

Collimator assembly

The F810SMA Series of fiber collimation packages is pre-aligned to collimate a laser beam propagating from the tip of an SMA-connectorized fiber with diffraction-limited performance at the design wavelength. Since the F810 Series fiber collimators do not have any movable parts, they are compact and not susceptible to misalignment. Due to chromatic aberration, the effective focal length (EFL) of the doublet lens is wavelength dependent. As a result, these collimators will only perform optimally at the design wavelength. The doublet lens is factory aligned so that it is one focal length away from the fiber tip when inserted into the collimator. This distance is equal to the focal length of the aspheric lens at the design wavelength. In addition, the doublet lens has an AR coating that minimizes surface reflections.

Ruled diffraction grating

These replicated, ruled diffraction gratings are offered in a variety of sizes and blaze angles. Ruled gratings typically achieve higher efficiencies than holographic gratings due to their blaze angles. Efficiency curves for all of these gratings are shown on the Figure 7. Absolute Efficiency

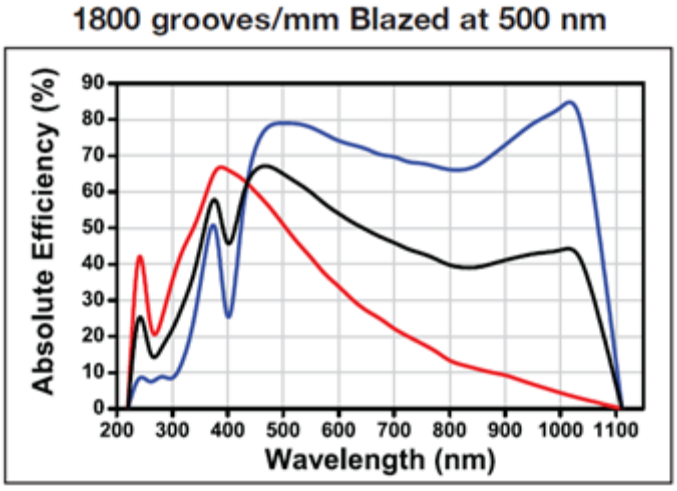

Figure 7. Absolute Efficiency

Concave mirror

Concave Mirrors offer high reflectance in broadband applications where the chromatic aberration introduced by a lens is not acceptable. When used close to 0° angle of incidence to collect and focus light for imaging applications, these mirrors provide >90% reflectance with the

metallic coatings and >99% reflectance with the dielectric coatings. Spherical Concave Mirrors are defined by the focal length, f, of the optic being half of its radius of curvature, R. To achieve the best performance without the introduction of off axis aberrations, concave mirrors should be used close to 0° angle of incidence.

Specifications

- Focal Lengths: 12 mm – 500 mm
- Substrate Material: N-BK7
- Reflective Coatings: Metallic and Dielectric Coatings
- Clear Aperture: >90% of Diameter
- Front Surface Irregularity: <λ/4 at 633 nm
- Front Surface Quality: 40-20 Scratch-Dig
- Back Surface: Fine Ground
- Diameter Tolerance: +0.0/-0.2 mm
- Thickness Tolerance: ±0.2 mm
- Chamfer: 0.25 mm @ 45° Typical

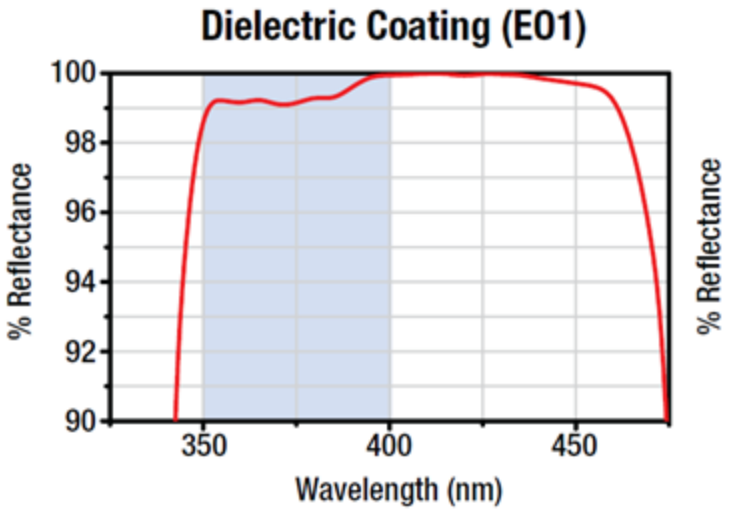

Figure 8. Reflectance of diffraction grating versus wavelength.

In Figure 8. Reflectance of diffraction grating versus wavelength. the shaded region represents the specified region for each coating. However when used at near 0° AOI, as is

recommended for a concave mirror, the wavelength range where the mirror has a high reflectance is significantly larger as can be seen in the performance

Optical filters

Longpass filters offer unprecedented performance in filter applications. The steep edges (measured from an optical density of 6.0 to a transmission of 50%) make it possible to measure even the smallest Raman shifts.

The large bandwidths and exceptional transmission permit these filters to be used in even the most demanding imaging applications.

One benefit of these laser filters, the rejected laser source light is reflected, easing stray-light management issues associated with holographic notch filters. Eliminating the need for complicated light baffling simplifies system design, creating more compact, cost-effective instrumentation. Second enhancing feature of these filters, with guaranteed transition widths (measured from the laser wavelength to the 50% transmission wavelength) of <1%, angle-tuning is unnecessary, greatly simplifying system setup and implementation. And finally, the coating process ensures unrivaled laser filter lifetime and durability, and guarantees "near-zero" temperature dependence, ensuring low long-term cost of ownership and maximum system operational range and sensitivity. These laser filters are not intended for general purpose longpass applications, as they do not have consistent blocking in the shortwave region.

Specifications

- Attenuation OD: 6
- Clear Aperture (mm): 21.3
- Filter Type: Longpass Filters
- Attenuation Range (NM): UV - Cut-on
- Exact Wavelength: 520
- Description: 520LP
- Brand: 3rd Millennium
- Peak T%: ≥ 90

- Cut-on (nm): 520
- Thickness (MM): 5.5

Figure 9. CAD of optical benchshows CAD of optical bench and assembly with PMT enclosure (upper panels) and assembly of spectrometer bench, PMT and PCB (lower panel).

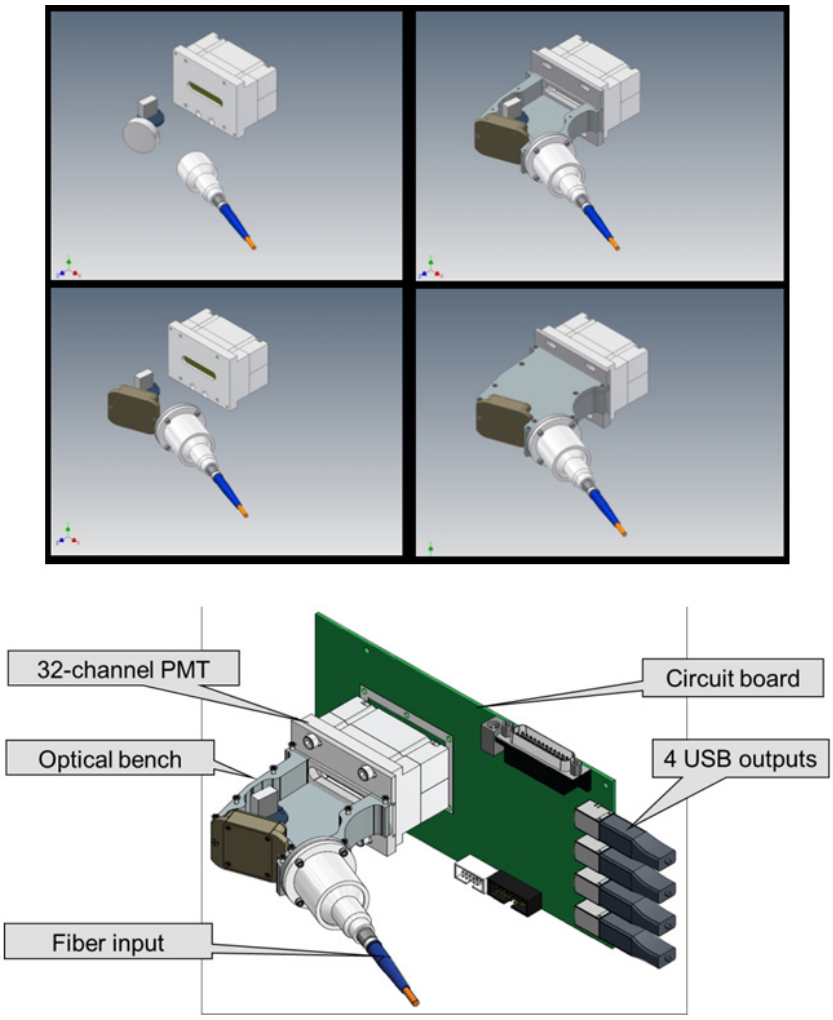

Figure 9. CAD of optical bench

As can be seen, the optical bench caries diffraction grating mounted on a fixture which has adjustable angle, Spherical mirror in a housing, fiberized collimator, and PMT housing with adjustable position. Lower panel of Figure 9. CAD of optical bench shows how optical bench is assemble with PCB. The PCB contains channel pulse amplifiers, 32-channel USB photon counter and has 4 USB outputs.

Figure 10. Block diagram and CAD of spectrometer assembly shows block diagram and CAD of the spectrometer assembly.

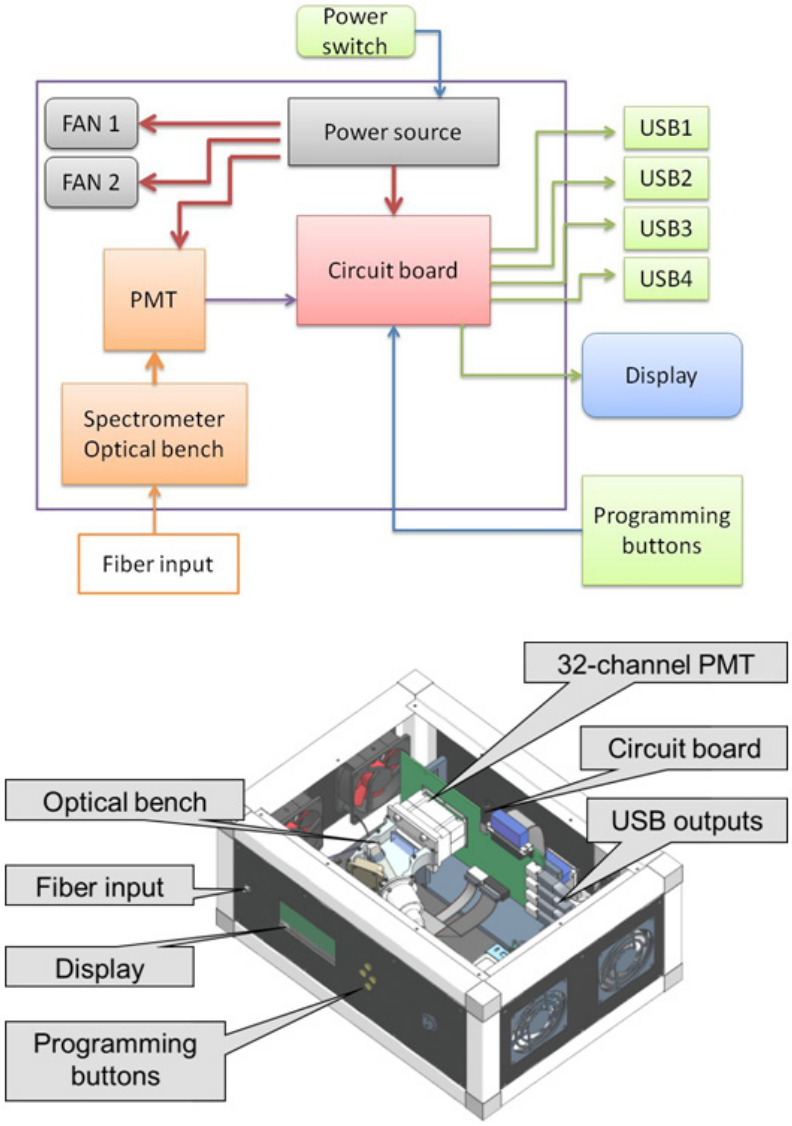

Figure 10. Block diagram and CAD of spectrometer assembly

The spectrometer assembly comprises a stabilized dc power supply (NES-100-5), which has voltage output 5V and maximum current 20A. Same voltage output supports two fans, PMT and used for supporting the PCB. The device is controlled by programing buttons which allow choosing different detection and recording regimes. The display shows the chosen operation regime. Optical signals are delivered to the spectrometer via input 200μm fiber.

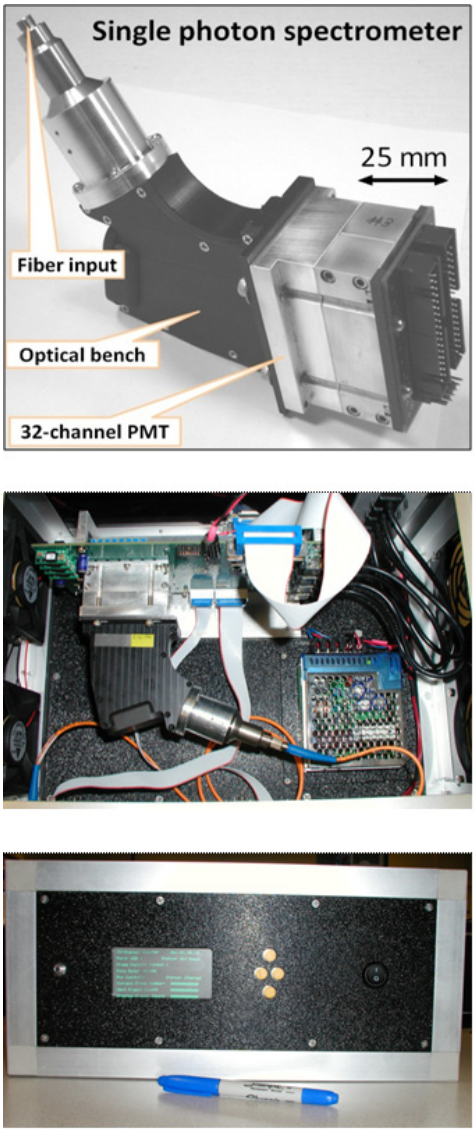

Figure 11. Photographs of the spectrometer

Figure 11. Photographs of the spectrometer shows the finalized spectrometer. Upper panel presents a photograph of the optical bench assembly, inner view of the spectrometer assembly is shown on middle panel, and general view of the spectrometer is presented on lower panel.

1.4.Testing of 32-channel single photon spectrometer

In order to characterize the spectrometer we connected the input fiber of the spectrometer to a monochromator (Figure 12. Block-diagram of the spectrometer characterization setup) and carried out measurements of the spectrometer response to different wavelengths.

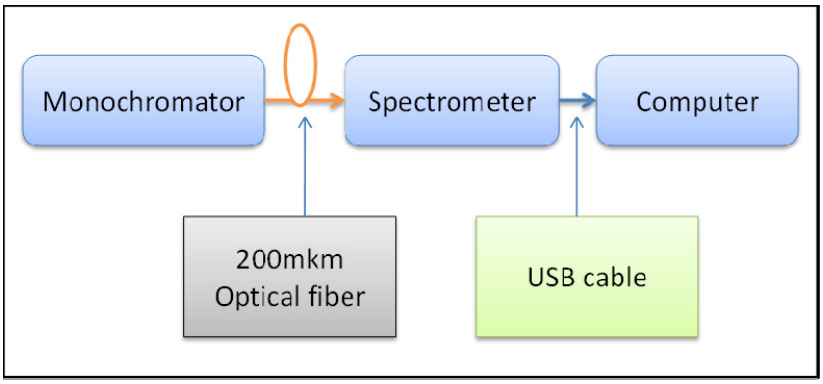

Figure 12. Block-diagram of the spectrometer characterization setup

Figure 1.4.2 presents channel resolution (upper panel) and wavelength resolution (lower panel) of the spectrometer with 32-channel PMT sensor. As can be seen, wavelengths which differ by 10nm are mostly detected by one channel of the PMT. Lower panel of the Figure 1.4.2 shows the wavelength resolution of the sensor. As can be seen, each PMT channel detects wavelengths in the range of ~10nm.

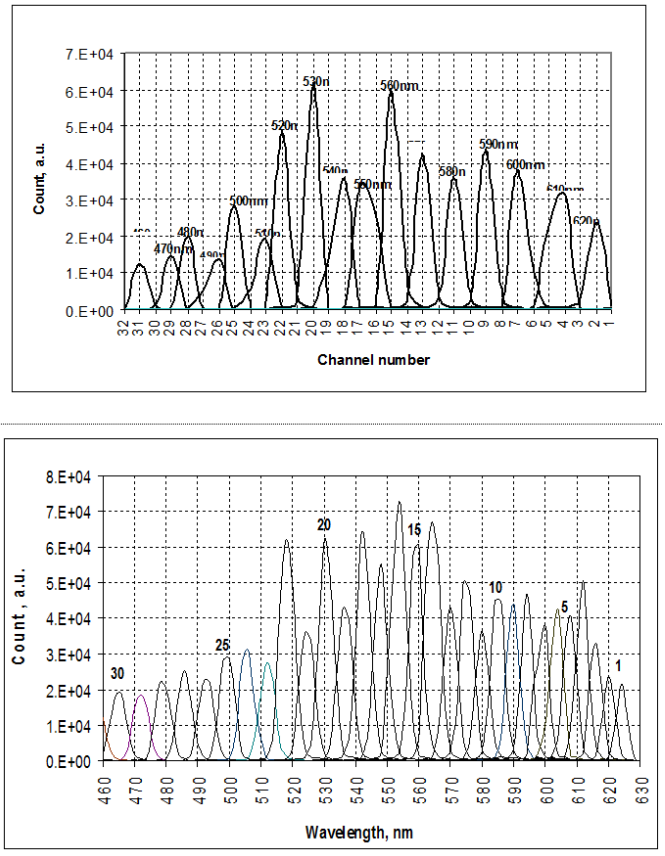

Figure 13. Spectral resolution of the spectrometer

Analysis of the spectral separation module of the spectrometer shows that it can provide spectral resolution as high as 1nm. The obtained spectral resolution of ~10nm is determined by the geometry of the 32-channel PMT which comprises 0.8mm×7mm detection zones separated by 0.2mm distance.

The overall resolution of the sensor can be improved by using an array of photoreceiving fibers connected to single photon sensors (Figure 14. Spectrometer with array of photo-receiving fibers (400mkm core, 650mkm pitch, upper and middle panels)) and wavelength resolution (lower panel).).

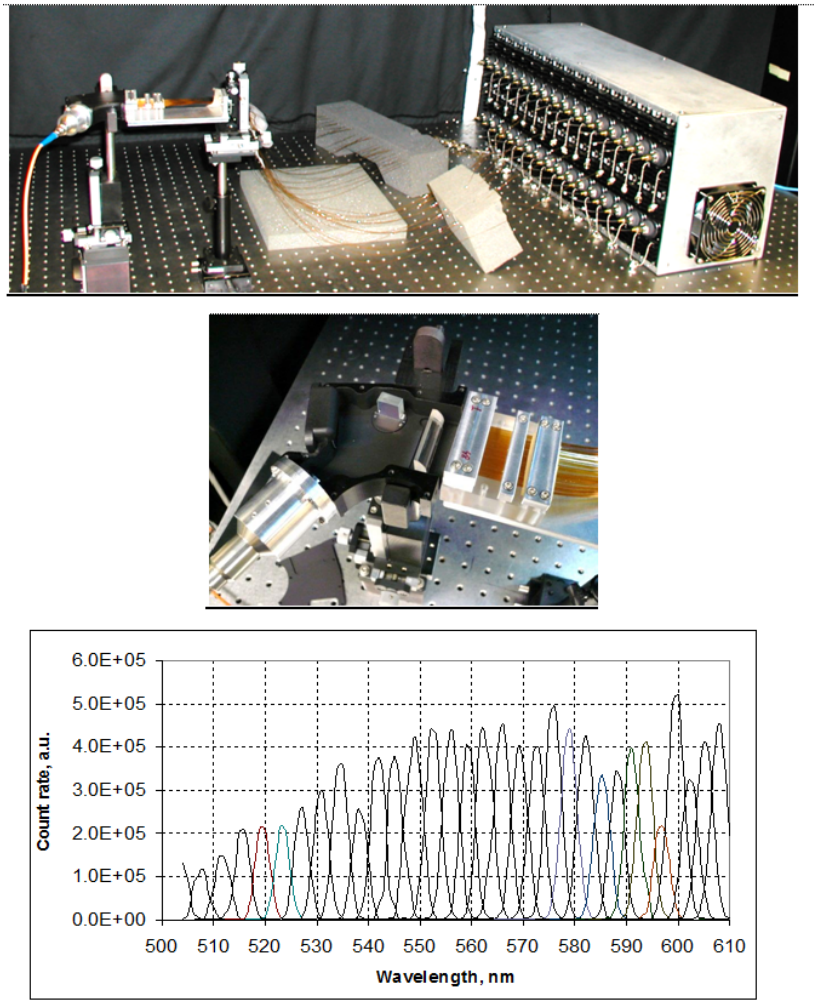

Figure 14. Spectrometer with array of photo-receiving fibers (400mkm core, 650mkm pitch, upper and middle panels)) and wavelength resolution (lower panel).

As can be seen on the lower panel of Figure 14. Spectrometer with array of photo-receiving fibers (400mkm core, 650mkm pitch, upper and middle panels)) and wavelength resolution

(lower panel)., the spectral resolution of the spectrometer with the fiber bundle is ~5nm. In fact, it means that the receiving fibers can be used as band pass filters in some applications when high spectral resolution is required.

CHAPTER 2. CAPILLARY FLUORESCENCE ANALYZER

2.1.System objective and key specs

The mail goal of the capillary fluorescence analyzer is to deliver fluorescence labeled sample from a sample tube to the fluorescence detection system. The analyzer can be used for measurements of fluorescent fluids, fluorescence-labeled micro- and nano-particles, and capillary electrophoresis

Key specifications of the sample analyzer include:

- Detecting up to 10,000 objects/s
- Minimized (less than 1%) beads loss and damage
- Sample contacts only with disposable parts of the analyzer (no equipment conservation needed)
- Volumetric speed up to 10μl/min
- Sample volume 2-150μl
- 1 μl dead volume
- Various types of beads (spectral range 520nm-720nm)
- Multi-laser excitation

2.2.Operation principle

Schematic of the analyzer is presented in Figure 15. Sample analyzer.

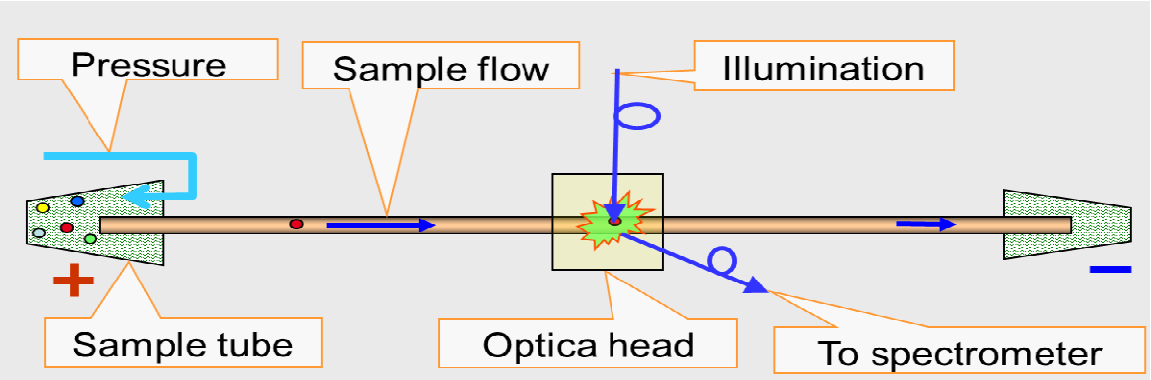

Figure 15. Sample analyzer

In the sample analyzer, fluorescent objects (molecules, micro-beads) are moved from a sample tube into a capillary by applying either pressure or electric field (electrophoresis). The pressure may be applied by either using fluidic system or compressed air. The capillary is inserted into a fiberized optical head (Figure 16. Schematic of optical head).

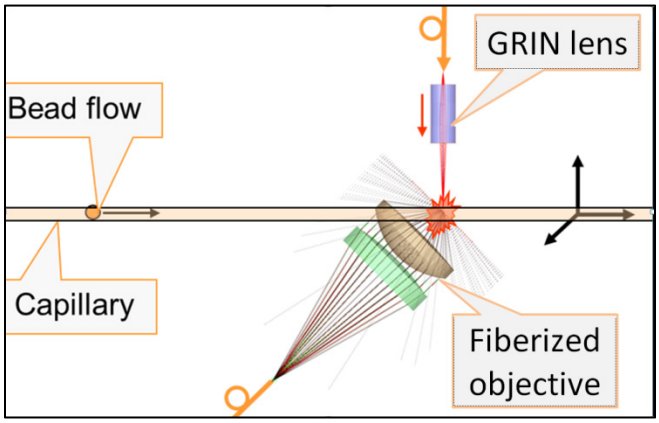

Figure 16. Schematic of optical head

Illumination from the fiberized laser module is delivered to the optical head and focused through a GRIN lens inside of the capillary. When fluorescent object passes through the laser beam, the excited fluorescence is collected by a fiberized micro-objective and delivered to the fiberized spectrometer, which records fluorescence with single photon sensitivity in 32 spectral

ranges between 500 and 720 nm. The data acquisition speed may be as high as 32MB/s at the frame rate of 1,000,000/s.

2.3.System with fluidic pumping

The purpose of fluidic system is to move samples diluted in liquid substance such as water, various buffers, alcohol, etc. though capillary with constant speed. Design of the fluidic system is shown in Figure 17. Schematic of analyzer with fluidic pumping.. Using 3-way flow switching valve (Upchurch, V-101L) we first move the sample from the sample tube into the pumping syringe (upper panel). From the syringe the sample can be pumped through the capillary (lower panel). When the sample is pumped through the capillary it passes the detection head and fluorescence of the sample is detected. The main advantages of this system are its ability to create high pressure which allows to move objects in the capillary at high speed (up to 1m/s in 25µm capillary), and very accurate pressure control, which allows supporting constant pressure (and speed) through the entire measurement process.

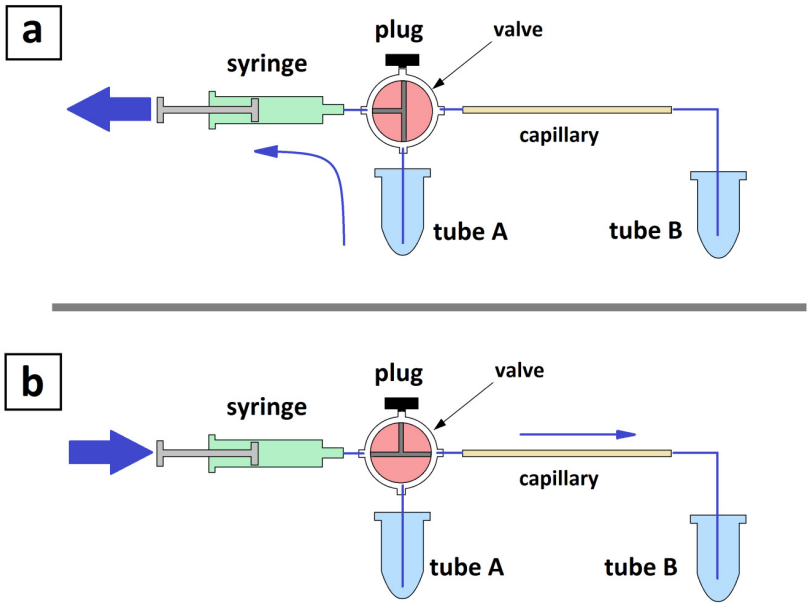

Figure 17. Schematic of analyzer with fluidic pumping.

In the course of use of the fluidic pumping system we found a number disadvantages when it is used for measurements of micro-objects (beads). The main reason here is that fluids containing beads are moving through a number of valves and tubing connectors. As a result, the

beads can stick to the walls of the tubing, connectors, and inner walls of the valves. This causes a number of major problems. Firstly, the beads which are captured in the valve, damage the valve which ultimately leads to the valve leakage, and also accumulation of the beads in the tubing clogs the system. Second problem is the bead loss itself. Indeed, it is practically impossible to obtain reproducible results because the bead count may change significantly from run to run.

Another disadvantage of the fluidic pumping is that the tubing causes a large dead volume of the system, which requires larger amount of sample.

Therefore our conclusion regarding the fluidic pumping is that this method is good for clear fluids and does not work well with suspensions.

2.4.System with air pressure pumping

In order to avoid disadvantages of the fluidic pumping, I have designed the capillary system with air-pumped sample. The main concept of the system was to avoid any contact of the sample with pumping system. In other words, from the sample tube, the sample should go directly to the capillary.

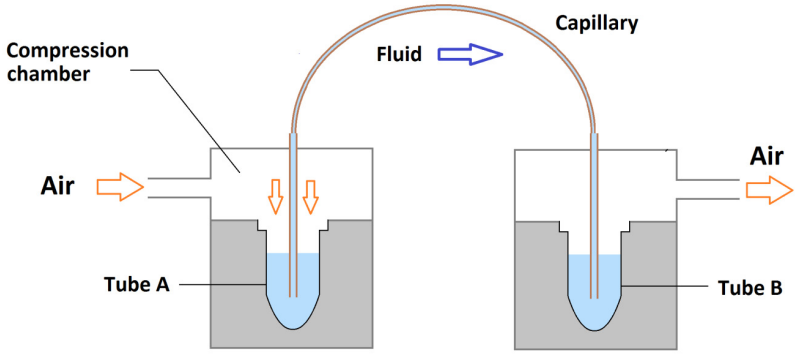

Figure 18. Schematic of air-pumped analyzer

Schematic of the air-pumped system is shown in Figure 18. Schematic of air-pumped analyzer.

Sample placed in the tube A and sealed in compression chamber. Compressed air enters into compression chamber and creates pressure on the surface of fluid. Fluid moves through capillary into a waste tube B. Left and right side of the system are symmetric. This design makes

possible pushing fluid in both directions by applying air pressure to a left or right input of the fluidic system. It allows, if needed, repeating measurements of the same sample.

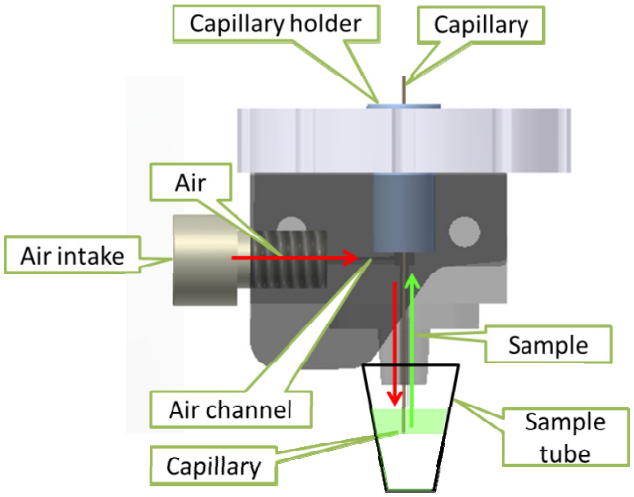

Figure 19. Detailed design of the compression chamber.

The most complex part of the system is the compression chamber. The complexity of this part is cause by (**i**) a requirement of sealing the sample directly in the standard sample tube, and (**ii**) also by the necessity of easy replacement of the capillary. A detailed design of the compression chamber is presented in Figure 19. Detailed design of the compression chamber.. In the chamber we have T-shape air channel through which air is pumped by a pumping syringe. The capillary is inserted into the chamber and fixed tightly by the capillary holder. Sealing of the chamber volume is done by (i) an airproof connection of the capillary holder with the body of the chamber, and by (ii) pressing the sample tube to the bottom of the chamber. Due to pumping, high air pressure (up to 150psi) is created in the chamber. When the capillary inlet is immersed into the sample tube the sample moves into the capillary due to high air pressure in the chamber.

Figure 20. CAD model (upper panel) and photograph (lower panel) of the air-pumped sample analyzer. presents 3D CAD model and photographs of the manual sample analyzer.

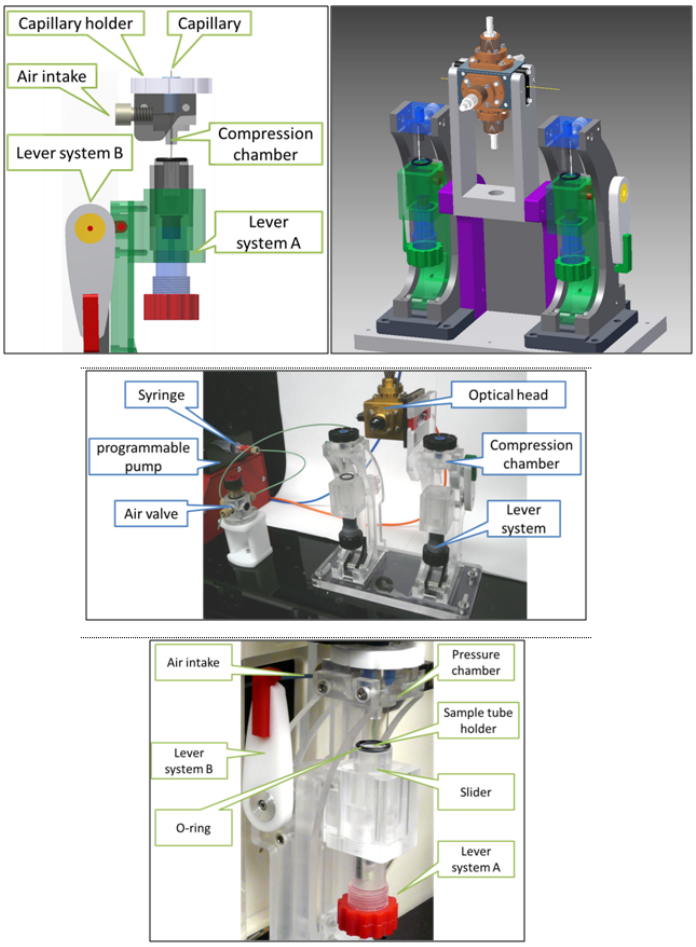

Figure 20. CAD model (upper panel) and photograph (lower panel) of the air-pumped sample analyzer.

The analyzer comprises two equivalent compression chambers connected by the capillary. The chambers are sealed by pressing the sample tube to the bottom surface of the chamber using the lever system. The capillary is passed through the fiberized optical head (see next section for details). The air is pumped using 5ml syringe mounted on the programmable pump. Using the air valve, pumping can be performed in both directions. The sample tubes are placed on mounts and using a lever system pressed against the compression chamber, so that the sealed air volume is created.

Because in the system, the analyte goes from the sample tube directly to the capillary, this design has minimum loss of particles during the run. The system design is such that it requires minimum cleaning because all parts that have contact with sample are disposable. Another advantage is minimum dead volume; it means that almost the entire sample volume can be pumped through the capillary.

The use of the syringe pump may cause pressure degradation in cases when sample volume is comparable with the sealed volume of the compression chamber. In this case, the volumetric pumping speed will decrease and this may cause some inaccuracy in measurements. In such cases a compressor which can support the required air pressure must be used.

Some factors add complexity to the design and fabrication of the air-pumped analyzer. Indeed, compression chamber has to be thoroughly sealed, even smallest air leak creates pressure degradation that reduces volumetric speed at which the beads move through the capillary. Another challenge is to design a chamber which is able to hold the required pressure (150psi in our device). Since gases are easily compressible, the volume of the chamber should be as small as possible. Compression chamber also has to be easy re-sealable to enable replacement of sample tubes.

2.5.Fiberized optical head

In the fiberized optical head the collection optics, the illumination optics, and the capillary are positioned along XYZ axes. Figure 21. Ray tracing in optical head presents ray tracing in the optical head.

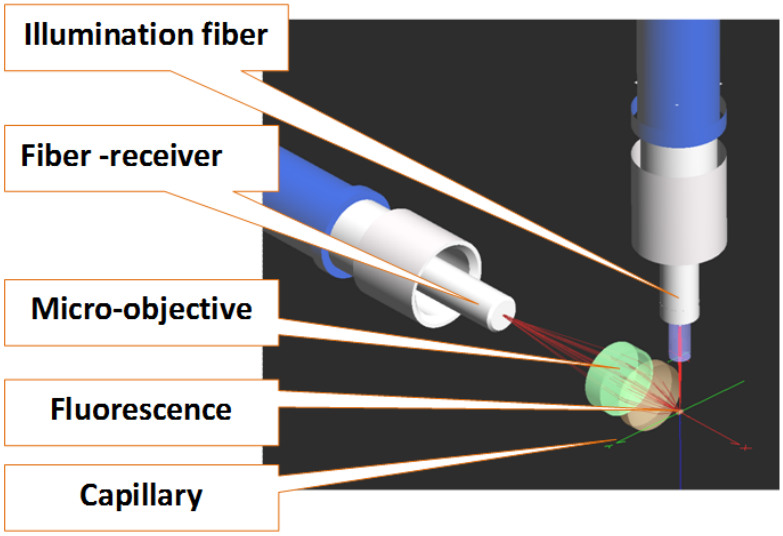

Figure 21. Ray tracing in optical head

Spectral properties of optical head

Spectral properties of the optical head are very important for accurate decoding of color-encoded beads. Indeed, when the bead is moving through the capillary, it may cross the laser beam along different trajectories (Figure 22. Beads in the capillary.).

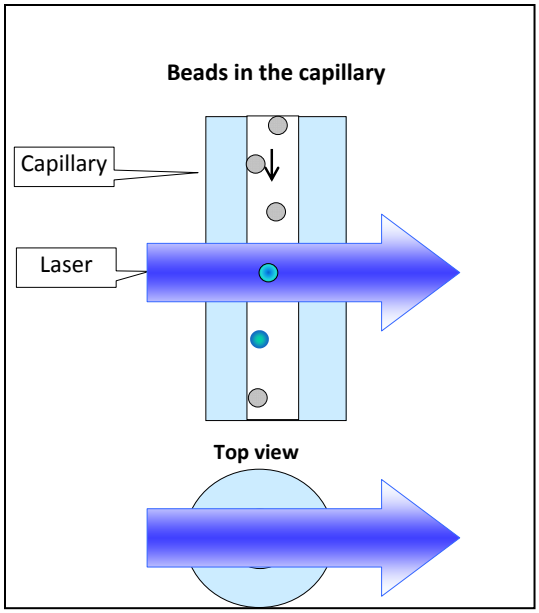

Figure 22. Beads in the capillary.

Depending on the trajectory, the fluorescence collection efficiency may differ. Moreover, the collection efficiency may depend also on the wavelength of the fluorescence, and these dependences may differ for different wavelengths. Figure 23. Mutual positions of the capillary, collection optics, and fiber-receiver in the optical head. presents schematic of mutual positions of the capillary and collection optics in optical head (the capillary goes along Z axis).

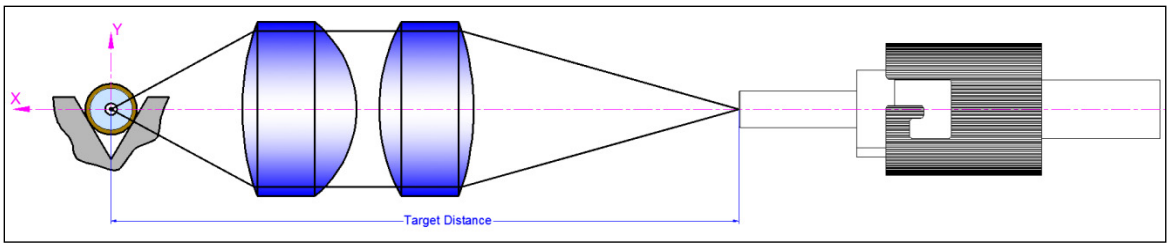

Figure 23. Mutual positions of the capillary, collection optics, and fiber-receiver in the optical head.

Upper and middle panels of Figure 24. Simulation of fluorescence collection efficiency for bead in capillary. (200μ collection fiber). Full ray tracing (upper panel), enlarged ray intercept area (middle panel), collection efficiency (lower panel). show results of ray tracing for three wavelengths (520nm, 620nm, and 720nm) for the bead positioned in the center of the capillary cross section (X=0, Y=0).

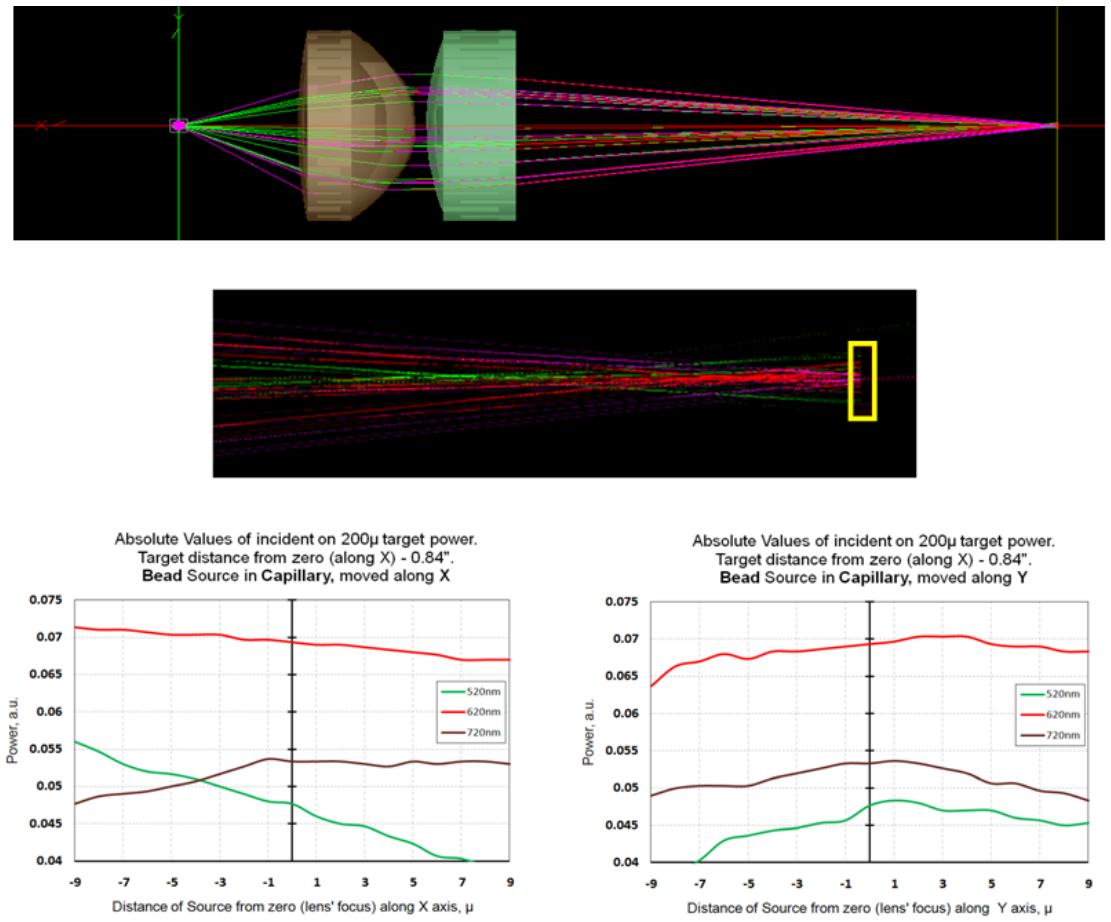

Figure 24. Simulation of fluorescence collection efficiency for bead in capillary. (200µ collection fiber). Full ray tracing (upper panel), enlarged ray intercept area (middle panel), collection efficiency (lower panel).

As can be seen, focus distances differ for all three wavelengths (middle panel). This is why collection efficiency of the fiber-receiver will depend on the wavelength. When fluorescent beads go along the capillary, their XY coordinates vary within diameter of the capillary. Obviously, position of the bead in the capillary influences it's focusing in the collection system. This is why fluorescence collection efficiency depends on both wavelength and position of the bead (Figure 24. Simulation of fluorescence collection efficiency for bead in capillary. (200µ collection fiber). Full ray tracing (upper panel), enlarged ray intercept area (middle panel), collection efficiency (lower panel)., lower panel).

The presented situation tells that the decoding of color-encoded beads will depend on trajectories of the beads in the capillary. As can be determined from calculations, the inaccuracy in determination of color code may be as high as 10-15%.

Figure 24. Simulation of fluorescence collection efficiency for bead in capillary. (200µ collection fiber). Full ray tracing (upper panel), enlarged ray intercept area (middle panel), collection efficiency (lower panel). presents results of simulation of fluorescence collection efficiency in 200µ collection fiber using achromatic collection lenses. As can be seen, from the ray tracing, with achromatic objective all wavelengths are focused in the same position (upper and middle panels).

Fluorescence collection efficiencies do not depend on wavelengths, but the use of achromatic optics yields absolute collection efficiency 2.5-3 fold lower than in the previous case (lower panel).

Our calculations also show that dependence of collection efficiency on fluorescence wavelength varies for different diameter of collection fiber (Figure 25. Simulation of fluorescence collection efficiency for bead in capillary (400µ collection fiber).).

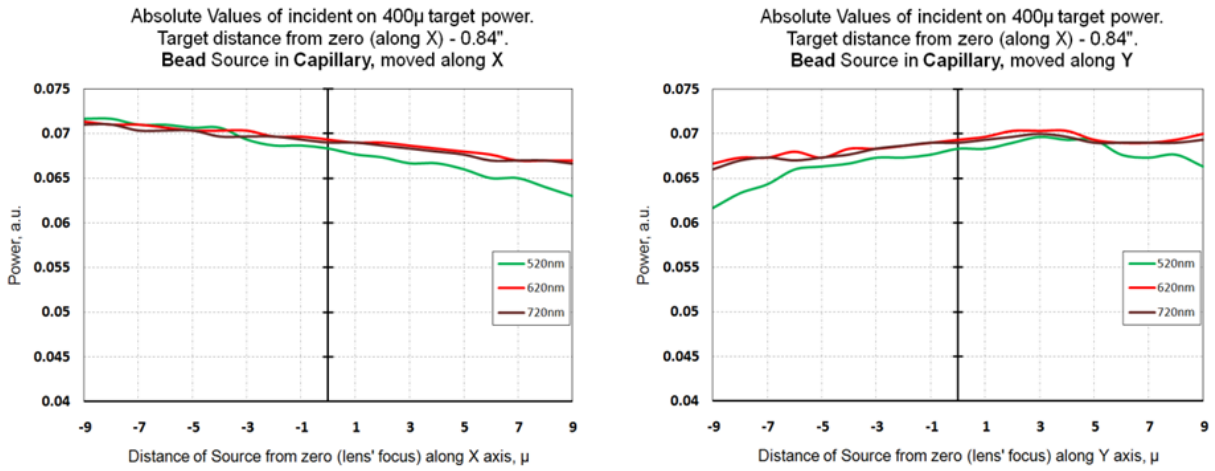

Figure 25. Simulation of fluorescence collection efficiency for bead in capillary (400µ collection fiber).

However, the use of 400mkm collection fiber is undesirable because it reduces spectral resolution of the spectrometer very significantly.

2.6. Testing of the bead reader

Volumetric speed depending on:

- Capillary diameter – 25mkm (20cm lengths) speed in water is 2mkl/min

- Capillary diameter – 50mkm (20cm lengths) speed in water is 30mkl/min
- Capillary diameter – 50mkm (55cm lengths) speed in POP-7 gel is 8mm/min

  Loss of beads less than 1%

Characterization detection accuracy

We have carried out characterization of the accuracy and the reproducibility of measured ratios of fluorescent signals obtained from groups of identical beads labeled with two dyes.

In order to check the accuracy of bead detection, we have assembled a special measurement setup (Figure 2.6.1 upper panel), which allowed us to control lateral position of the capillary in the optical head as well as to rotate the capillary around its axis. Using a high precision positioning system, the capillary was moved so that beads were illuminated individually by the laser beam, and multiple measurements of the same bead in a fixed position were performed and recorded. Figure 2.6.1 (middle panel) shows a distribution of photon counts measured from an individual bead (see also a red area in Figure. 2.6.1 (lower panel)). As can be seen, the

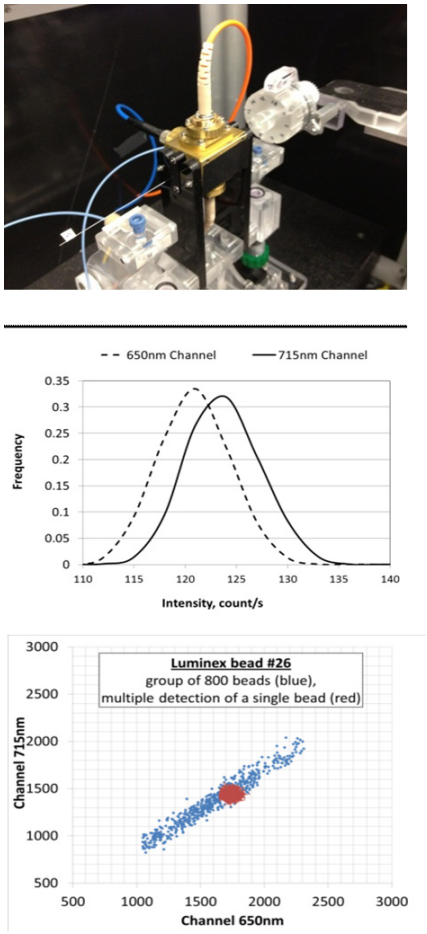

Figure 26. Measurement setup for determination of bead detection accuracy (upper panel), distribution of photon counts measured from individual bead immobilized in the optical head (middle panel), and a bead map of a set of Luminex beads (lower panel)

distribution is Poissonian (*mean is equal to variance*), which is characteristic of photon counting. Thus, we conclude that the accuracy of our measurement system is limited by photon counting noise, which is a fundamental limit. Figure 26. Measurement setup for determination of bead detection accuracy (upper panel), distribution of photon counts measured from individual bead immobilized in the optical head (middle panel), and a bead map of a set of Luminex beads (lower panel) (lower panel) presents a bead map obtained for a group of ~800 Luminex beads (blue dots) in comparison with multiple measurements of a single bead, which was immobilized in the optical head (red dots).

A large (~2-fold) spread of measured photon counts from individual beads (blue dots) is due to a non-uniform distribution of the laser beam in the capillary. However, the ratio of photon counts

obtained in two spectral channels is almost constant, and it varies mostly due to the photon counting noise (see red zone indicating single bead measurements).

CHAPTER 3. APPLICATIONS

3.1.Measurement of composition of fluorescent dyes

Figure 27. Schematic of the measurement setup. presents a schematic of the setup for measurements of fluorescence spectra of multicolor fluorescent analytes in capillary. In the setup, the analyte is moved from a sample tube into the capillary by either electrophoresis or air pressure. The capillary is inserted into a fiberized optical system. Fluorescence in the analyte is excited by Ar-ion laser (488 and 514 nm, Uniphase, CA, USA), collected by the fiber (200μ core diameter) and delivered to the spectral separation module of the spectrometer.

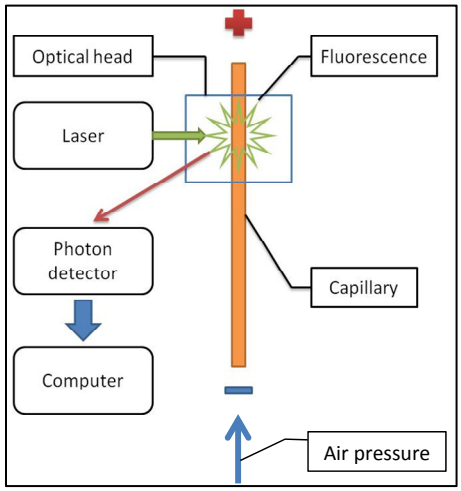

Figure 27. Schematic of the measurement setup.

Our task in this application is to determine composition of several fluorescent dyes which are mixed in a single sample. In order to do this we measure fluorescent spectra of individual dyes using our measurement setup, and then use known spectra for determination of content of individual dyes in the analyzed mixture.

The experimental setup records optical fluorescence spectra in 32 independent channels of the PMT. Each sample represents the full spectrum of fluorescence in the range from 460 to 630 nm. The range is divided among the PMT channels so that each channel collects fluorescence in a 5-10 nm band.

Fluorescence from an individual dye is simultaneously measured by several PMT channels. Photocount rate is distributed among PMT channels according to fluorescence spectrum of the dye. In practice, the measured distribution of photocount rates is influenced by

differences in sensitivity between channels and optical cross-talk. In order to ensure reliable operation, the system must be calibrated for a particular dye set. During the calibration some unit concentration of each dye of the set is presented to the system and its spectrum is recorded. The set of spectra is used to estimate optimal parameters of signal processing (see [Tsupryk A., 2008]). Detailed description of color decomposition method is also presented in [D. Gudkov et all, 2012, submitted to Biosensors & Bioelectronics].

Measurements of mixtures of quantum dots

In order to test the sample analyzer, we have carried out measurements of mixtures of three different types of QDs with strong spectral overlap (Figure 28. Spectra of individual quantum dots.). QDs re-suspended in toluene 1mg/ml were obtained from Crystalplex, Pittsburgh PA.

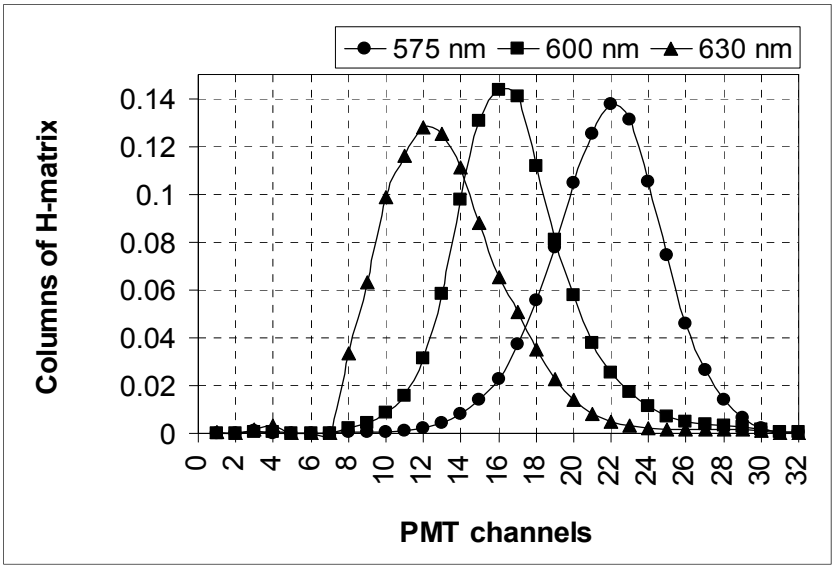

Figure 28. Spectra of individual quantum dots.

We premixed QD solution consisting of 50% of 575 nm QDs and 50% of 630 nm QDs and prepared a subsequent series of mixtures in which the content of 600 nm QDs varied from 0% to 15%. Mixtures of quantum dots were pumped into fused silica capillaries with transparent coating (360 μm OD, 100 μm ID, Polymicro AZ, USA) and detected using the setup presented in Figure 3.1.1. The total recording time for each mixture was about 5 minutes with minimum integration time of ~20 ms which provided approximately 15,000 data points per mixture. The color deconvolution procedure described D. Gudkov, 2012, was applied to photo-counts obtained

in 32 channels at each data point during 20 ms photon integration time. In order to increase the photon integration time, we summed photo-counts obtained from several sequential data points and thus applied the color deconvolution procedure to longer time intervals.

Based on the measured spectra of individual QDs we have carried out color deconvolution procedure. The obtained results are presented in Figure 3.1.3. As can be seen from Figure 3.1.3 (left), the concentration of the 600 nm QDs determined from the fluorescence measurements is practically equal to the original concentration of that component in the prepared QD mixtures. Figure 29. Deconvolution of QD mixtures (left) and distributions of concentrations of 600 nm QD determined with 0.1 s and 0.02 s integration times (right). (right) presents distribution of concentration of the 600 nm QDs recovered from multiple measurements of the mixtures with 0.1 s and 0.02 s integration times. As can be seen, increase of the integration time improves the resolution of QD mixtures.

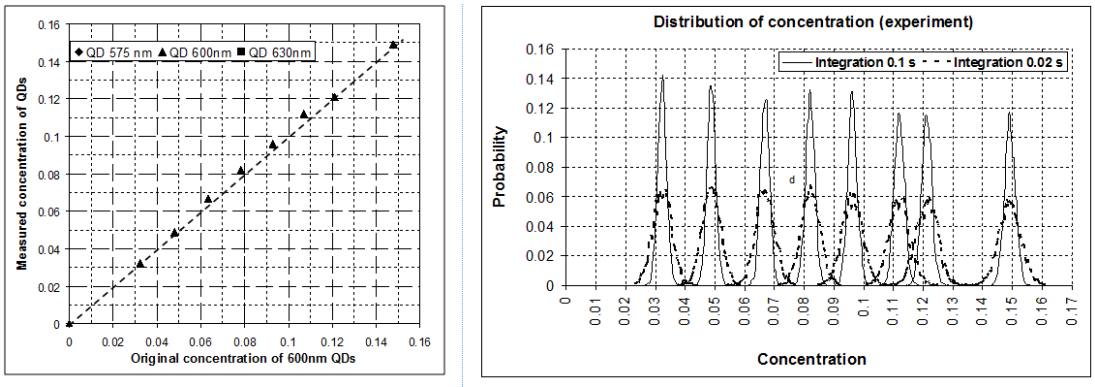

Figure 29. Deconvolution of QD mixtures (left) and distributions of concentrations of 600 nm QD determined with 0.1 s and 0.02 s integration times (right).

Based on the analysis of distributions of color compositions obtained experimentally found that distribution of measurements is Poissonian, and the accuracy is determined by square root of the obtained photon count.

As can be found from Figure 29. Deconvolution of QD mixtures (left) and distributions of concentrations of 600 nm QD determined with 0.1 s and 0.02 s integration times (right)., the developed sample analyzer can resolve dye mixture with precision of ~3%, which is very important for measurements of color-encoded objects (see next section).

3.2.Measurement of color encoded beads

Beads encoded with combinations of up to 5 types of quantum dots

Characterization of QDs

Five types of QDs (525nm, 540nm, 580nm, 630nm and 665nm) were purchased from CrystalPlex Corp, Pittsburgh, PA. Schematic of the setup used for characterization of QDs is presented in Figure 30. Emission spectra of five QDs.. Illumination of the capillary was done by single mode lasers [*Ar-ion, (488nm and 514nm), solid state (532nm), and semiconductor (638nm)*]. We found that the excitation by Ar-ion laser (*25µm beam, 25mW output power*) was optimal for all QD types. Stock solutions of QDs (8µM) were diluted 1:5000 and run through 50µm ID capillary. The obtained QD spectra are shown in Figure 30. Emission spectra of five QDs.

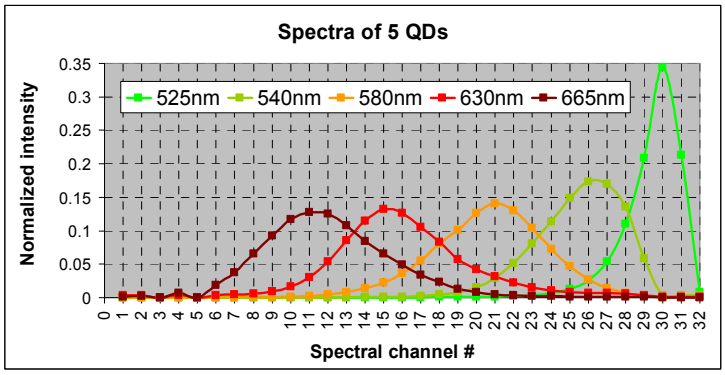

Figure 30. Emission spectra of five QDs.

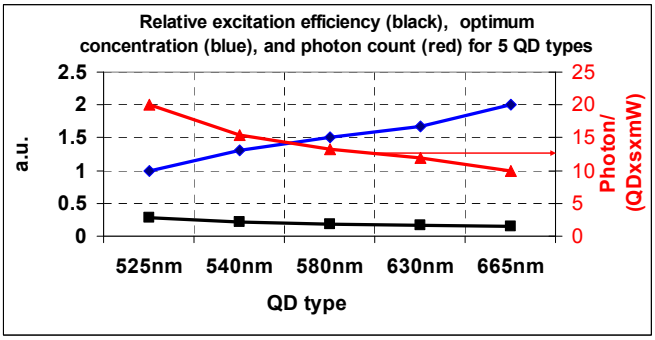

Figure 31. Excitation efficiency, optimum concentration and photon count for 5 QDs of five QDs.

For each QD type we have measured the photon yield (*a number of photons emitted by one QD in the maximum spectral channel per second per 1mW of illumination power,* Figure 31. Excitation efficiency, optimum concentration and photon count for 5 QDs of five QDs., red curve). Based on the relative excitation efficiency of all studied QD types (Figure 31. Excitation efficiency, optimum concentration and photon count for 5 QDs of five QDs., black curve), we

have determined the optimum relative concentrations of QDs which provide equal photocount rate for all five QD types (Figure 31. Excitation efficiency, optimum concentration and photon count for 5 QDs of five QDs., blue curve). All calculations were done based on the illuminated volume of the capillary (~31,000 cubic microns), concentration of QDs in the solution, and the illumination power (*25mW from Ar-ion laser*).

Characterization of beads 5μm, single color porous beads doped with 525nm, 540nm, 580nm, 630nm, and 665nm QDs were purchased from CrystalPlex Corp, Pittsburgh, PA.

Imaging of the beads showed that the variation of beads' diameter did not exceed 20%.

Saturation of the beads According to the manufacturer, the number of QDs which saturates the bead can be as high as ~2million. Based on the determined excitation efficiencies for of QDs and targeting equal fluorescence signal from each QD type, we have calculated a maximum number of QDs per bead for sets of beads encoded with 2-, 3-, 4- and 5 QD types (Figure 31. Excitation efficiency, optimum concentration and photon count for 5 QDs of five QDs.).

It is important to emphasize, that the number of QDs per bead may be limited by the linearity of the photon detector (10^8photon/s in our spectrometer) rather than by the saturation of the bead by QDs. Our estimates based on the measured photon yield of QDs show that for 25mW excitation power the number of QDs per bead may not exceed ~250,000.

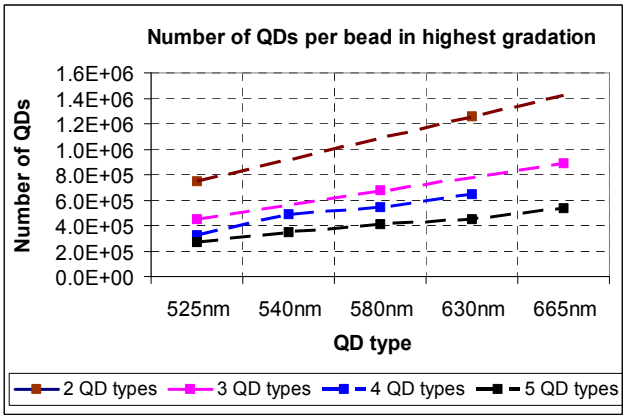

Figure 32. Emission spectra of five QDs.

Testing statistically encoded beads

According to the determined specifications, 2-, 3-, 4-, and 5- color sets of randomly encoded beads were fabricated for us by CrystalPlex Corp.

In order to assess quality of the random coloring technology, we introduced two major characteristics for the set of beads: (***i***) a number of distinguishable codes in the set, and (***ii***) distribution of random codes on the color map (*in the phase space of color codes*).

(***i***) ***Determination of distinguishable codes***

We call a bead unique (having a distinguishable code), if its color code differs *significantly* from codes of all other beads in the set. In this case, once detected, the unique bead becomes identifiable by its color code in all subsequent detection events.

<u>*Criterion for recognition of the beads and assigning accuracy to the bead decoding*</u> In order to distinguish two statistically encoded beads, we introduce a parameter called "code distance" $\boldsymbol{D_{12}} = \sqrt{\sum_{i=1}^{N_{QDS}} \left(\boldsymbol{C_{i1}} - \boldsymbol{C_{i2}}\right)^2}$, where $C_{i1\ and}\, C_{i2}$ are color codes of the two beads for i^{th} color component and $\boldsymbol{N_{QDS}}$ is a number of QD types used for encoding the beads.

In single photon spectrometer, the accuracy of the determination of the color code of the bead is limited by Poisson noise generated by fluorescence photons. Therefore, 99% of all measurements fall within the interval $\delta_{TH} = \pm 3\sigma$ where σ is standard deviation, which is related to the detected number of photons Φ as: $\sigma = \sqrt{\Phi}$. We consider codes of two beads distinguishable if the code distance $D_{1,2} > \delta_{TH}$ (1).

In order to determine experimentally parameter δ_{TH} we carried out multiple measurements of the same bead by fixing position of the bead in the capillary using liquid polymer matrix. We performed spectral measurements of the bead (Figure 33. Spectra of a single bead (upper panel), determination of bth (middle panel) number of distinct color combination (lower panel)., upper panel) and calculated the distances between codes obtained from all measurements. In order to determine δ_{TH} we have developed specialized software which calculates code distances between all beads in the set. Figure 33. Spectra of a single bead (upper panel), determination of bth (middle panel) number of distinct color combination (lower panel). , middle panel, presents a distribution of normalized code distances calculated for 4,000 measurements of a single bead. As can be seen, distances between the measured codes of the bead do not exceed 0.003 (which means that if the code distance between two beads exceeds 0.003, the beads are distinguishable with 99% accuracy).

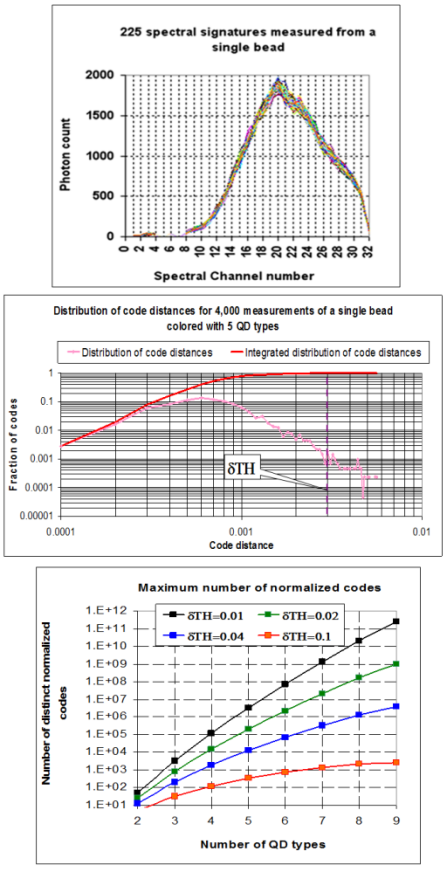

Figure 33. Spectra of a single bead (upper panel), determination of bth (middle panel) number of distinct color combination (lower panel).

Statistics of random codes, distribution of codes on color map

Number of distinguishable color codes

Using Monte-Carlo technique, we have calculated a number of distinguishable normalized color codes in sets of beads depending on the number of encoding QD types and δ_{TH} as a parameter. Results of computer simulations of the normalized color codes for randomly encoded sets of beads are presented in Figure 3.2.4, lower panel (components of a normalized color code present fractions of photon counts generated by each type of encoding QDs. Sum of all code components is always equal to 1).

Based on the obtained results, we conclude that for δ_{TH}> 0.003 one can potentially obtain up to 100,000 distinct color codes by using only 4 QD types and more than a million codes by using 5 QD types.

2-color sets of beads

Using the developed sample analyzer measurements of four 2-color random sets of beads: (525/540nm, 600/630nm, 540/580nm and 660/660nm) have been carried out and yielded similar results for all four sets. Based on the obtained δ_{TH}, we have found up to 40-50 distinguishable codes in the measured 2-color sets of beads. Typical color maps for absolute and normalized codes for 2-color set are presented in Figure 34. Statistics of color codes in 2-color random set (600nm/630nm). (left and middle).

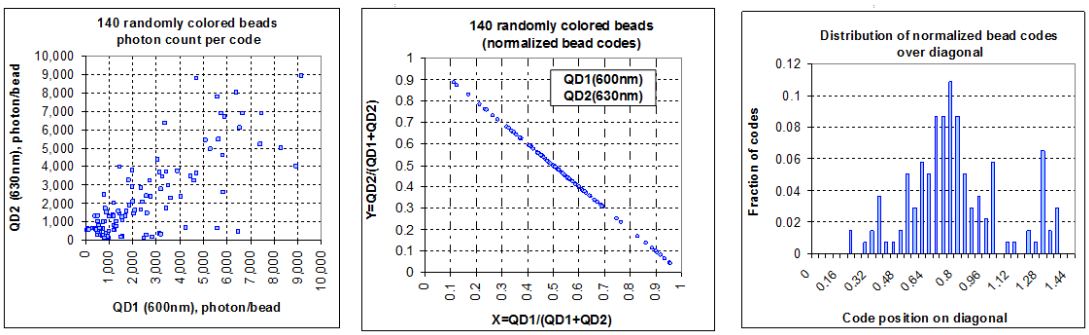

Figure 34. Statistics of color codes in 2-color random set (600nm/630nm).

Since the sum of normalized codes for any individual bead is always equal to 1, the color map for the normalized codes is a diagonal of the square (1, 1). The distribution of the normalized codes over the diagonal (Figure 34. Statistics of color codes in 2-color random set (600nm/630nm)., right) shows that the color map is filed with the codes rather unevenly. It means that in order to provide maximum number of codes predicted in Figure 34. Statistics of color codes in 2-color random set (600nm/630nm)., *right panel,* the coloring technology needs to be optimized, targeting more even distribution of the codes.

3-, 4-, and 5-color sets of beads

Typical distributions of codes measured for random sets of beads encoded with two and more QD types are shown on radial color maps (Figure 35. Upper panels: typical color maps for 2-, 3-, 4-, and 5-color random sets of beads. Lower panel: distribution of color codes experimentally obtained for 5-color set of 6,000 beads., *upper panels*). Each axis of the radial map presents one component of the normalized code. Individual beads are shown on the map as polygons whose sides connect values of the beads' codes on the axes of the map.

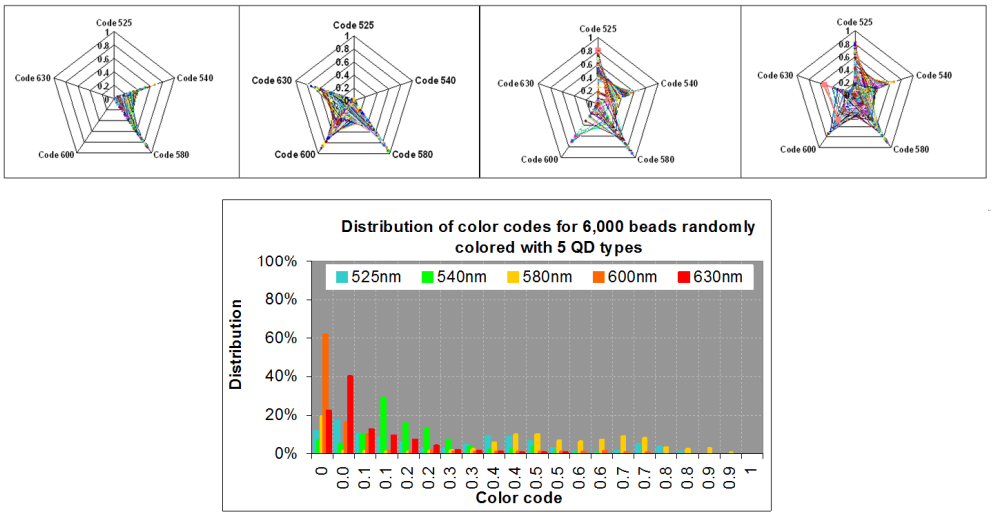

Figure 35. Upper panels: typical color maps for 2-, 3-, 4-, and 5-color random sets of beads. Lower panel: distribution of color codes experimentally obtained for 5-color set of 6,000 beads.

Lower panel of Figure 35. Upper panels: typical color maps for 2-, 3-, 4-, and 5-color random sets of beads. Lower panel: distribution of color codes experimentally obtained for 5-color set of 6,000 beads. shows a distribution of color codes measured for 5-color sets. This shape is typical for all studies sets of beads. As can be seen from the obtained data, the space on the color maps occupied by the codes of the beads covers only a small fraction of the map's area. Because of that, the number of distinguishable codes, obtained for the sets is smaller than maximum number of codes, which can be reached only if the entire color map is filled evenly with random codes.

Taking into account the experimentally determined δ_{TH}, we have been able to identify up to 40-50 distinguishable codes with 2-color sets; up to 150 codes with 3-color sets; up to 1,000 codes with 4-color sets; and more than 9,000 codes with 5-color sets.

Detection of color encoded beads from Luminex

In order to evaluate the accuracy of our system in the bead recognition, we have carried out experiments with commercial beads from Luminex (Microplex X-Tag Microspheres, Luminex, Austin TX, USA) which are internally labeled with 630 nm and 715 nm dyes having certain intensity levels of the two dyes. Figure 36. Spectra of Luminex dues and bead-map of 50 types of Luminex beads. shows spectra of two encoding dyes (left) and the bead-map obtained for 50 types of beads in 50 μm ID capillary (right).

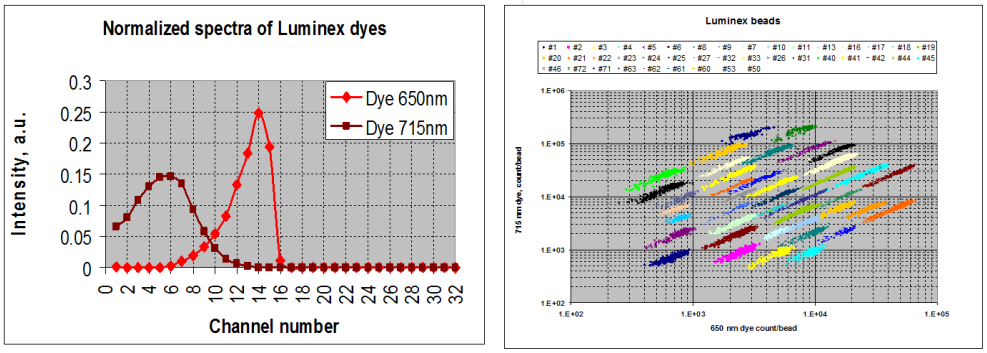

Figure 36. Spectra of Luminex dues and bead-map of 50 types of Luminex beads.

As can be seen, the areas occupied by different types of beads do not overlap. Accuracy of the code recognition is determined as a ratio of the correctly classified beads to the total number of the detected beads. Our data analysis showed that we could recognize up to 50 types of beads with 99% accuracy.

Typical color maps for two different sets of beads are shown in the Figure 37. Color maps obtained from two types of Luminex beads with two different ratios of 630 nm and 715 nm dyes. Upper and lower panels present 1:1 and 1:7 ratios, respectively. (*X and Y axes present photon count obtained from individual beads from 650 nm and 715 nm dyes respectively*).

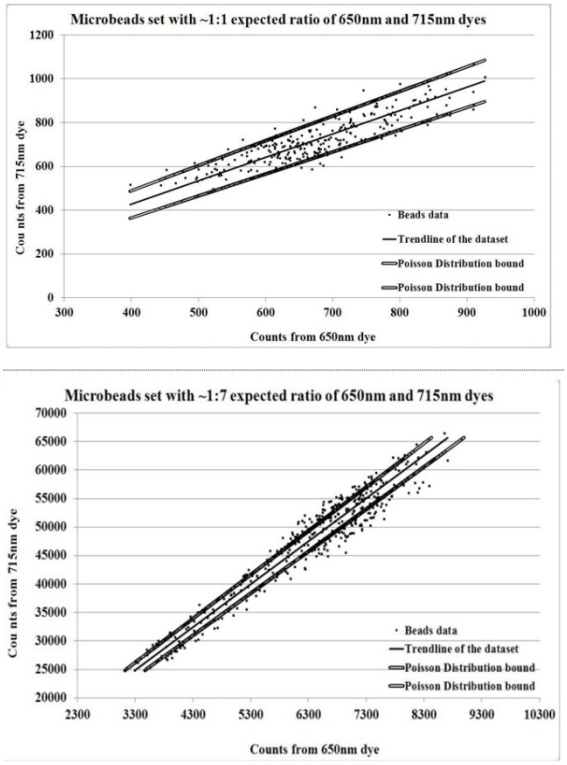

Figure 37. Color maps obtained from two types of Luminex beads with two different ratios of 630 nm and 715 nm dyes. Upper and lower panels present 1:1 and 1:7 ratios, respectively.

As can be seen, the beads of the same type are distributed along both axes which can be attributed to a non-uniform distribution of the laser power inside the capillary. Trend line represents the slope corresponding to the ratio of the two dyes. Double lines represent 3 standard ranges of deviation (3σ) from corresponding photon counts on the trend line. For both sets of beads one can see significant number of beads detected out of 3σ range, which in our opinion shows a non-uniformity in the bead coloring process.

3.3.DNA sequencing

DNA sequencing system

The developed sample analyzer was tested for DNA sequencing by capillary electrophopresis. Photograph and schematic of DNA sequencing system are presented in Fig.3.3.1. In order to perform DNA sequencing, 50cm, 50mkm ID capillary was filled with liquid polymer. In order to move DNA sample through the capillary, high voltage (8-15kV) was

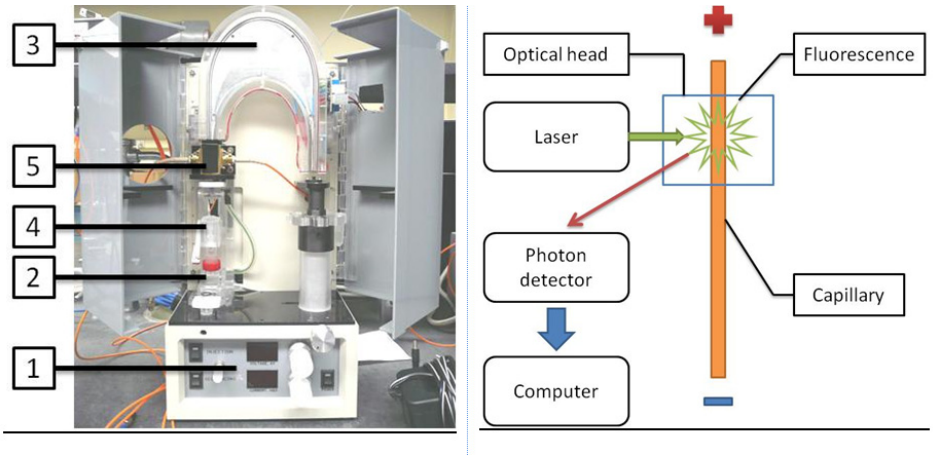

Figure 38. Photograph and schematic of the single lane DNA sequencer.

Right panel: sample analyzer modified for DNA sequencing. 1 - high voltage supply with a built-in voltmeter and ampermeter; 2 - polymer replacement system; 3 - temperature control system; 4 - tube-changer; 5 – fiberized precision optical system. Left panel: schematic of the optical system.

applied to the sample and the waste tubes. When the fluorescently labeled DNA fragments pass the optical system (B), they are illuminated by a fiberized laser (either Ar-ion laser (488 and 514nm, 20mW, Uniphase, CA, USA) or Nd:YAG laser (532nm, 25mW, GCL-025-S, CrystaLaser, NV, USA). The laser-induced fluorescence is collected by the fiber (200mkm core diameter) and delivered to the spectral separation module.

DNA sequencing chemistry and protocols

DNA samples labeled with BigDye (BigDye Terminator v1.1 Sequencing Standard) obtained from Applied Biosystems (Foster City, CA, USA) were denatured in 25 µl Formamide (Applied Biosystems) followed by dilution 1 to 5 in HPLC grade water immediately prior to injection. DNA separation was conducted at 150 V/cm in 40 cm (35 cm separation length) uncoated capillaries (50 µm inner diameter, 365 µm outer diameter from Polymicro, Phoenix, AZ, USA) filled with POP-7 separation medium (Applied Biosystems) at 50°C. Applied Biosystems running buffer was used.

Processing of DNA sequencing data

We tested two approaches to estimation of fluorescence intensities produced by four dyes used for labeling of A, C, G and T terminators: decomposition of the entire measured spectrum

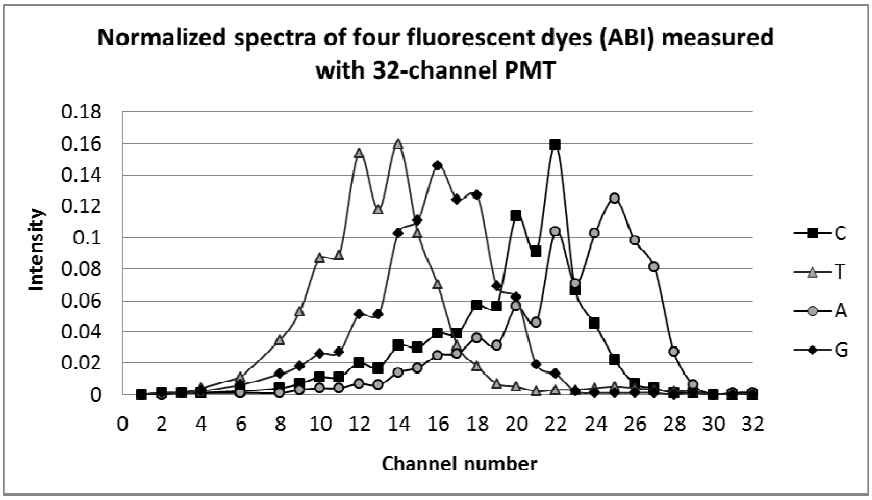

Figure 39. Spectra of labeled terminators measured by 32-channel spectrometer.

and application of virtual filters (see Tsupryk A. 2008 for signal processing details). For the *decomposition of the entire measured spectrum,* the spectra of individual dyes were obtained experimentally by measuring fluorescence emitted by each dye separately and by normalizing the measured vector of photocount rates (Figure 39. Spectra of labeled terminators measured by 32-channel spectrometer.).

The determination of concentrations of individual dyes in the mixture was performed for each time frame. The obtained sequence of dye concentrations forms four sequencing traces, which are further used for base calling.

The *method of virtual filters* is a simplified approach, which can be successfully used if the dye spectra a well separated. Four virtual filters are formed by selecting a certain PMT channels or groups of channels so that fluorescence of each dye contributes the most into measurements in the channel, which was assigned to it, and minimum response in the other channels. For the simplified data processing we selected 18, 15, 11 and 5 channels of the PMT for G, A, T and C correspondingly.

The obtained color de-convolution matrices for Ar-ion and Nd:YAG lasers are shown in Figure 40. System matrix C and color deconvolution matrices used for processing of DNA sequencing data.

Excitation	Ar-ion laser (488nm & 514nm), 18mW			
Base	**Color deconvolution matrix**			
G	1	0.842	0.297	0.124
A	0.147	1	0.366	0.264
T	0.007	0.104	1	0.809
C	0	0.008	0.057	1
Excitation	Nd-YAG laser (532nm), 17mW			
Base	**Color deconvolution matrix**			
G	1	0.679	0.254	0.084
A	0.416	1	0.285	0.179
T	0.009	0.253	1	0.493
C	0.025	0.024	0.109	1

Figure 40. System matrix C and color deconvolution matrices used for processing of DNA sequencing data.

In both data processing approaches the obtained four sequencing traces undergo standard processing [Alaverdyan L., 2002)].

It is important to emphasize that both approaches to the data processing yielded similar sequencing traces and base calling quality. However, for measurements characterized by small signal-to-noise ratios the first approach gives better results since it uses the entire information about the fluorescence emitted by each dye rather than just the fluorescence obtained in only four selected channels of the spectrometer (see Figure 41. Sequencing traces processed using full spectrum analysis (upper panel) and virtual filter approach (lower panel).).

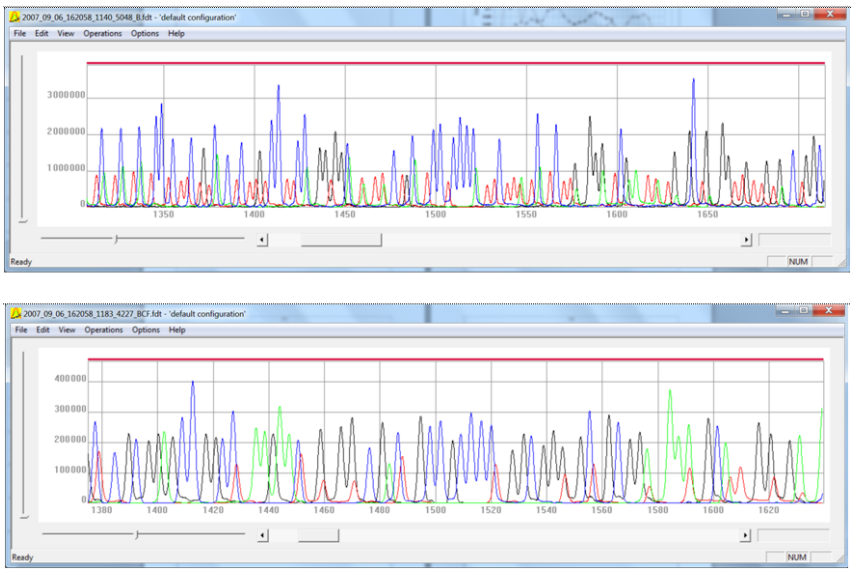

Figure 41. Sequencing traces processed using full spectrum analysis (upper panel) and virtual filter approach (lower panel).

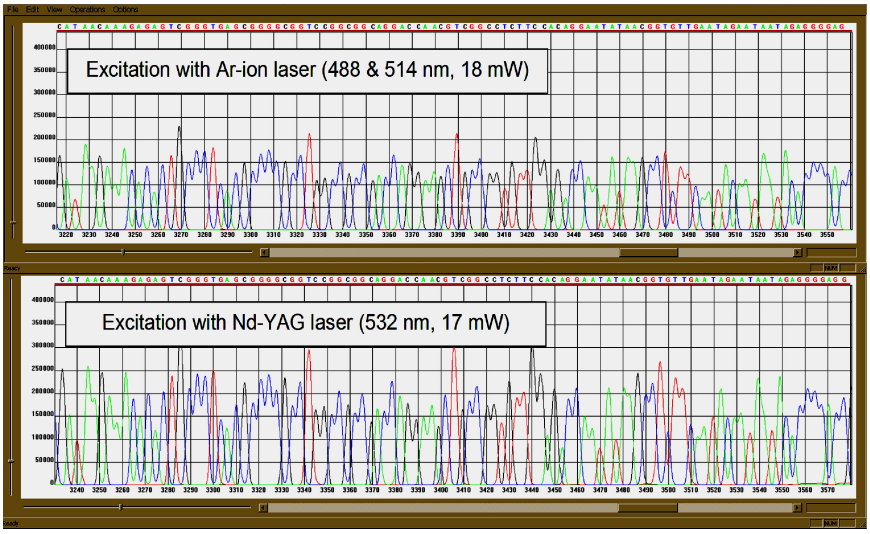

Figure 42. DNA sequencing traces obtained with Ar-ion and Nd-YAG lasers.

As can be seen, the signal obtained from virtual filter approach is almost 10 fold lower. Another advantage of using the entire fluorescence spectrum obtained from the dye is a significant increase of the detection dynamic range. Indeed, in our 32-channel photosensor the channels have linear response up to ~7×10^7photocounts per second and if the measured fluorescent dye has a broad spectrum, the linear range of the detection for this dye will be proportional to the number of simultaneously illuminated channels of the sensor.

Figure 42. DNA sequencing traces obtained with Ar-ion and Nd-YAG lasers. presents two DNA sequencing traces obtained the developed data acquisition system using single photon spectrometer and two lasers.

We found that sequencing traces recorded with the two lasers look very similarly and the quality scores are nearly identical. The obtained sequence read length is as long as ~650 base pairs which is in a very good agreement with the read lengths obtained for the same capillary length in commercial DNA sequencers (ABI-3730, AppliedBiosystems Inc., Foster City, CA).

CHAPTER 4.
FLUORESENCE ACTIVATED SORTINGRING OF THE BEADS WITH CNVs

4.1.Copy-number variations

(CNVs) are alterations of the DNA that results in the cell having a normal variation in the number of copies of one or more sections of the DNA. CNVs correspond to relatively large regions of the genome that are presented in fewer or larger number than normal on certain chromosomes. This variation accounts for roughly 1% of human genomic DNA and each variation may range from about one 1,000 bases to several mega-bases.

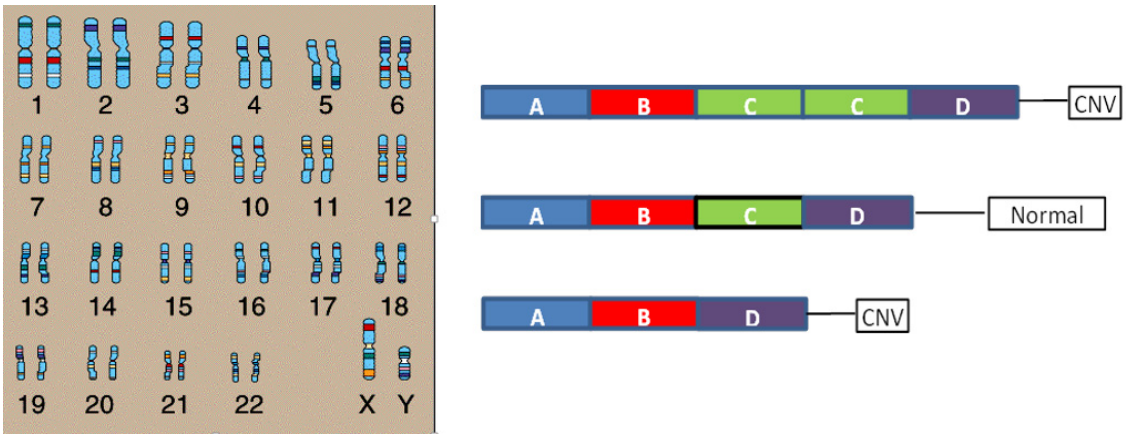

Figure 43 Left: Each human cell contains 23 pairs of chromosomes, which can be distinguished by size and by unique banding patterns. This set is from a male, since it contains a Y chromosome. Females have two X chromosomes. Right: A chromosome that normally has sections in order as A-B-C-D might instead have sections A-B-C-C-D (a duplication of "C") or A-B-D (a deletion of "C")

Our CNV detection technology includes the following steps:

A. Generation of water-oil emulsion with droplets containing beads and single fragments of cut genomic DNA (This step is performed using microfluidic chip)

B. Preparation of whole-genome templated library on beads by emulsion PCR

C. Hybridization of fluorescence-labeled genomic DNA from control and patient on the bead library

D. Fluorescence activated sorting of the beads which show ratiometric changes corresponding to CNVs.

I have considered capillary-based and chip based sorting system

E. Sequencing of DNA hybridized to the beads which carry CNVs, and creation of CNV data-base.

(This step will be done by high throughput DNA sequencing facility)

Background for CNV detection on beads

The idea of the CNV detection is shown in Figure 44 Two fluorescent markers are used to label separately control DNA, which does not contain CNVs, causative for disease, and DNA obtained from the patient. Labeled DNA is mixed in equal amounts and the mixed sample is hybridized on beads from genomic library, every bead carries certain region of DNA. After hybridization beads carry 2-color labeled DNA.

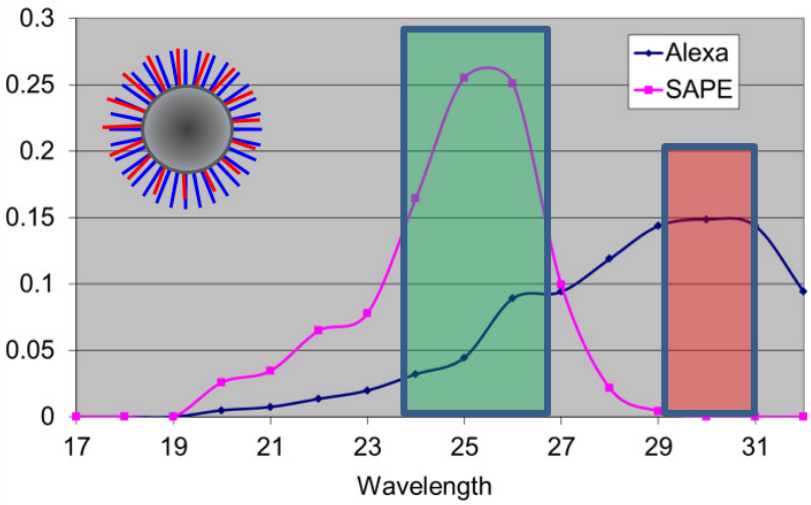

Figure 44 Two fluorescent markers are used to label separately control DNA, which does not contain CNVs, causative for disease, and DNA obtained from the patient. Labeled DNA is mixed in equal amounts and the mixed sample is hybridized on beads from genomic library, every bead carries certain region of DNA. After hybridization beads carry 2-color labeled DNA.

Proportion of two colors corresponds to the ratio R of labeled DNA in the mix. Ratio R shows difference in the amount of specific DNA regions in control and patient's DNA.

Schematic of bead sorting is shown in Figure 45. Schematic of the sorting system. Left panel: Laser beam illuminates the capillary and when the bead crosses the laser beam it produces fluorescence. The fluorescence is directed to multi-channel photon detector so that different

channels of the detector receive different ranges of fluorescent spectrum of the bead. Right panel: Front view of multichannel detector.

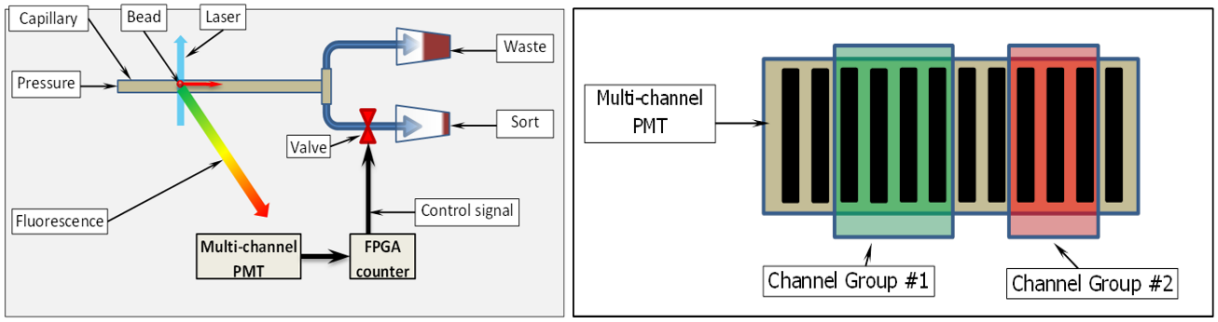

Figure 45. Schematic of the sorting system. Left panel: Laser beam illuminates the capillary and when the bead crosses the laser beam it produces fluorescence. The fluorescence is directed to multi-channel photon detector so that different channels of the detector receive different ranges of fluorescent spectrum of the bead. Right panel: Front view of multichannel detector.

4.2.Bead Sorting Criterion

For each group of channels we calculate entire fluorescent signal $\mathbf{F_1}$ and $\mathbf{F_2}$:

$$F_1 = \sum_{m_0}^{m_1} C_m ; \quad F_2 = \sum_{n_0}^{n_1} C_n ,$$

where $\mathbf{m_0}$ and $\mathbf{n_0}$ are the first channels and $\mathbf{m_1}$ and $\mathbf{n_1}$ the last channels in Channel Groups #1 and #2 correspondingly.

Depending on the ratio of photon counts in the two groups of channels ($\mathbf{R=F_1/F_2}$) we can distinguish the beads which we want to select (sort) from the beads which go to waste. Thus, if we want to sort out all beads with CNVs, we have to send to the waste all beads with ratio $\boldsymbol{R}$ =1:1 (no CNV).

When we measure beads which are labeled with the same ratio $\boldsymbol{R}$, the results have a spread which is caused by the measurement noise. So, actually measured ratios for individual beads with the same ratio fall within a certain range: $\boldsymbol{R1<R<R2}$ (Figure 46 Bead maps. Beads corresponding to 1:1 label ratio (left), bead corresponding to CNV label ratios (0:2, 1:2, 3:2, 2:2, 2:1, 2:3, 2:0).). Therefore, CNV-positive beads will have either ratios $\mathbf{R<R_1}$ or $\mathbf{R>R_2}$

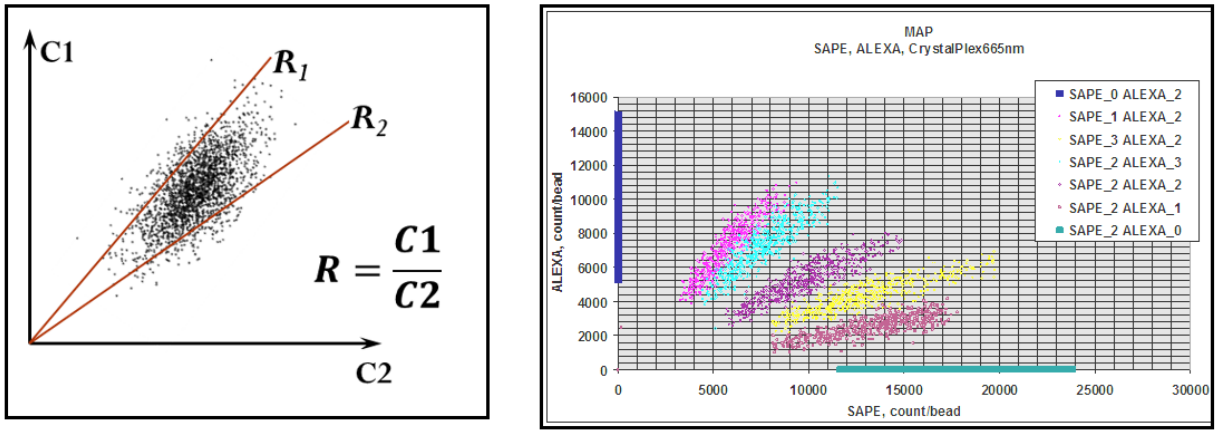

Figure 46 Bead maps. Beads corresponding to 1:1 label ratio (left), bead corresponding to CNV label ratios (0:2, 1:2, 3:2, 2:2, 2:1, 2:3, 2:0).

4.3.Design and development of capillary bead sorter

Principle of fluorescence activated sorting of the beads

My goal was development and testing of a micro-fluidic bead sorter based on the laser-induced fluorescence for copy number variation (CNV) analysis.

Typically size of CNV is larger than 1000bp. If we want to perform whole-genome detection of CNVs, we will have to detect ~1,000,000 objects. Thus, detection time is very important. Our system can detect up to 10000 bead/s. Since CNVs constitute ~1% of the entire genome, we will need to perform ~100 sorting/s. This is a big challenge because of the slow nature of mechanical sorting. Therefore we suggested to sort beads by cyclic enrichment.

The main idea of our approach is to perform CNV sorting by cyclic enrichment of the beads of interest. The approach to sorting is based on two facts: (i) DNA samples usually contain only small percentage of CNVs and (ii) speed of the bead detection is much higher than the sorting speed.

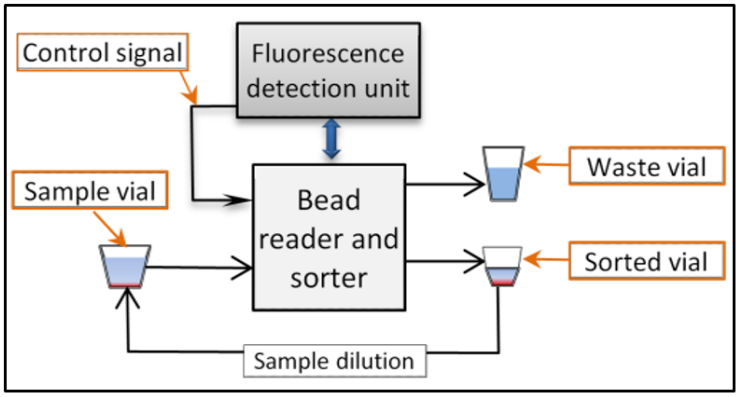

Figure 47 Block diagram of the sorting method

The sample which contains two types of beads characterized by two color ratios in their fluorescent spectrum is moved from the sample vial to the bead reader (CNVs, shown in red). When beads which carry CNVs pass through the detection zone, the fluorescence detection unit generates a control signal which activates the sorting event. The sorter directs CNV-positive beads to the sorted vial and other (blue) beads go to the waste vial. Because sorting speed in the system is always lower than the detection speed, a certain fraction of blue beads gets into the sorting vial at every sorting event. After the cycle of sorting is completed, the detection system which counts beads and sorting events, determines the enrichment of CNV beads: $E = N_{CNV\ beads} / N_{beads}$ in sorting vial.

If **E** is lower than the required enrichment, the sample from the sorted vial is diluted to the volume of the original sample, and next sorting cycle is performed. We have already determined two other types of solenoid valves from Lee Company which have 2ms and 0.25ms response time (http://www.theleeco.com/LEEWEB2.NSF).

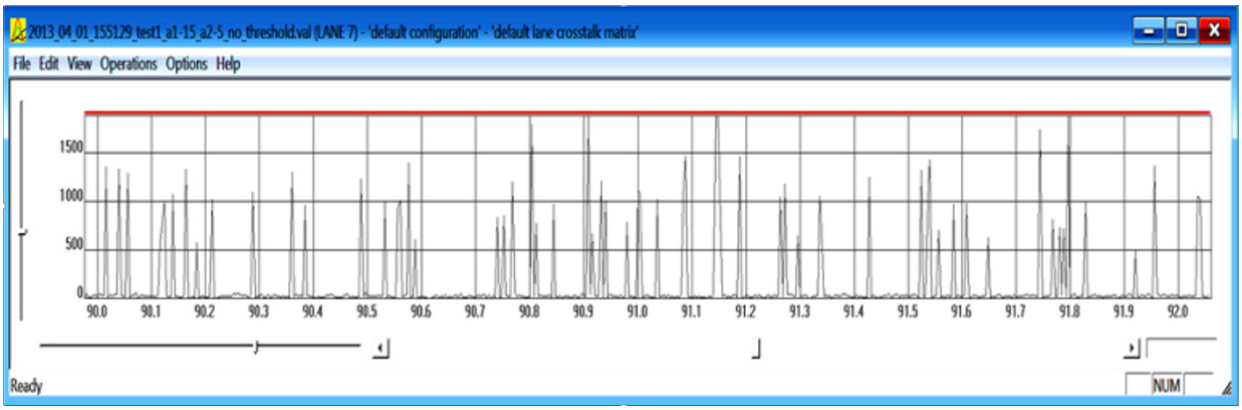

Figure 48 Screenshot Beads

Development of capillary-based fluorescence activated bead sorter

Figure 49. CAD model (upper panel) and implemented capillary bead sorter (lower panel). presents models of solenoid valves (upper panel) used and photograph (lower panel) of the implemented bead detector/sorter. As sorting valve we have chosen solenoid valves from Lee, Westbrook, Connecticut 06498-0424 U.S.A. We used models 075P2NO12 and INKX051185A with valve switching times ~20ms and 0.2ms correspondingly.

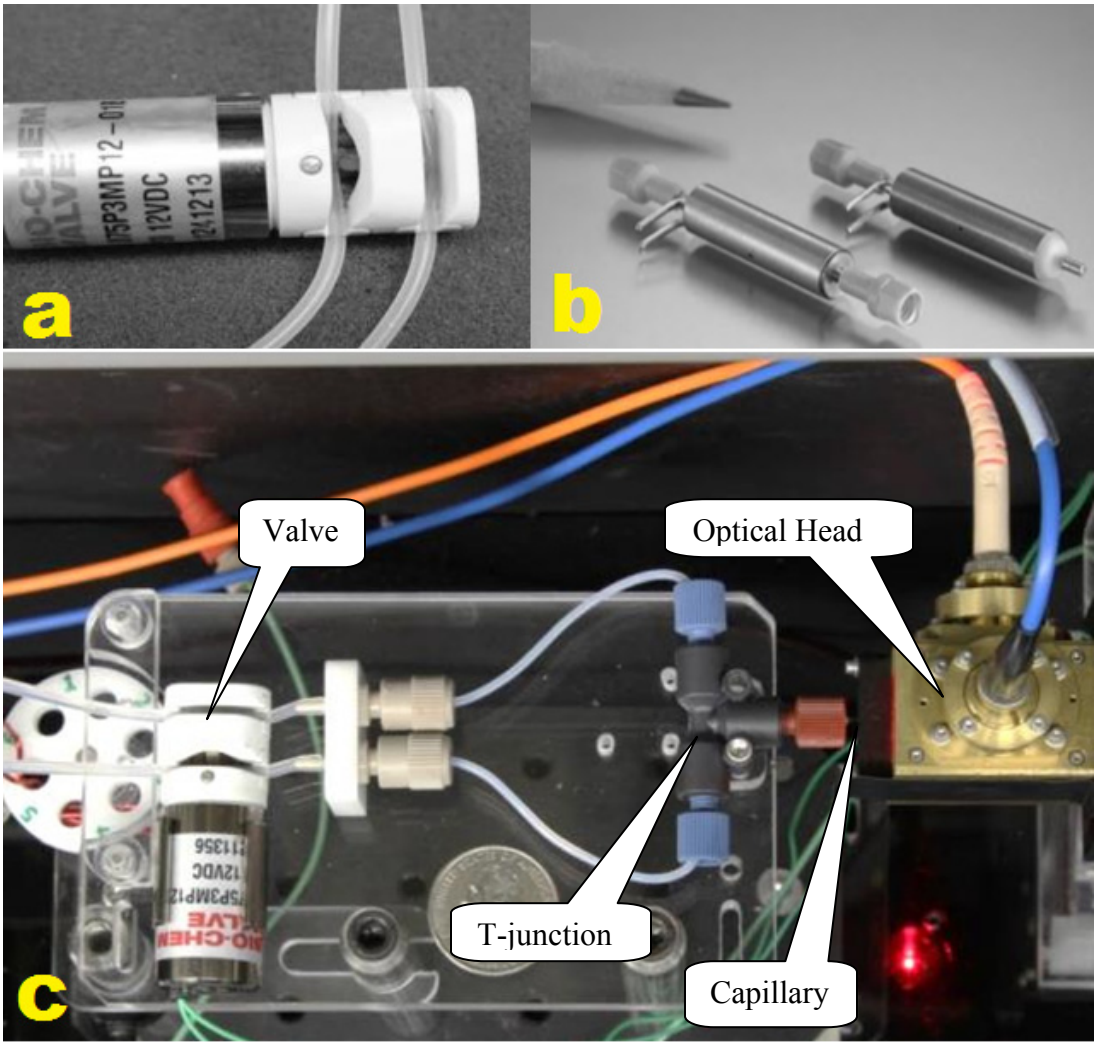

Figure 49. CAD model (upper panel) and implemented capillary bead sorter (lower panel).

Fig.50 presents CAD model of the sorting system. In this system sorting of the beads is performed using in T-junction in conjunction with solenoid valve. The sample tube with beads is

placed in the Air Chamber and the beads are injected into a fused silica capillary (320mkmOD and 50 -100mkm ID) which is inserted into the optical head.

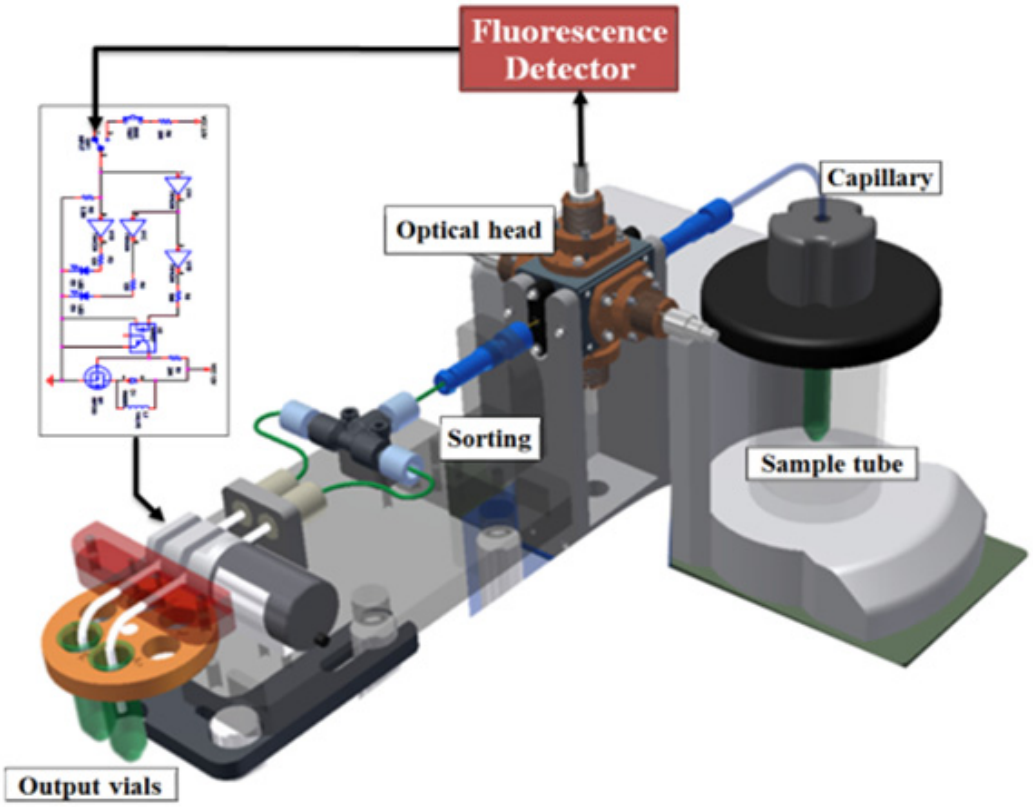

Figure 50

Individual beads are detected in the optical head, and depending on their labeling the detection unit sends a control signal to the valve (the valve control circuit is shown in the corner). The valve, which normally keeps the waste channel opened, closes the waste channel and opens the sorting channel.

Fig. 51 and Fig. 52 present block-diagram and schematic of the valve control unit.

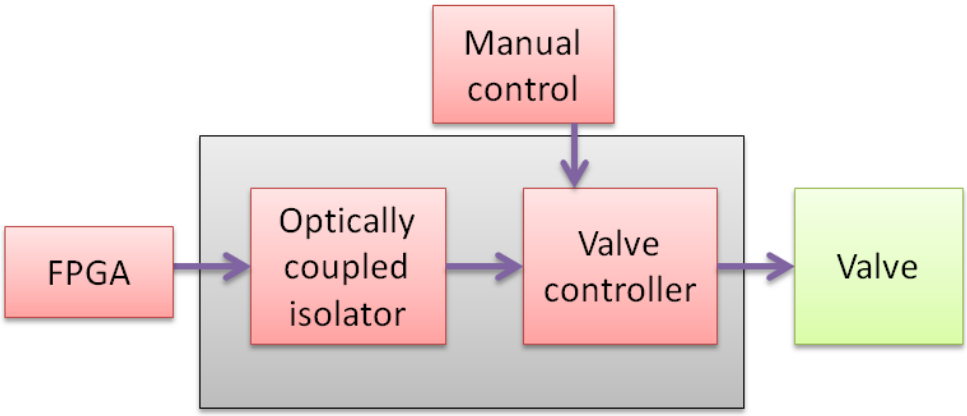

Figure 51 Block diagram of valve control unit.

The valve control circuit is shown in Figure 52 Valve control circuit

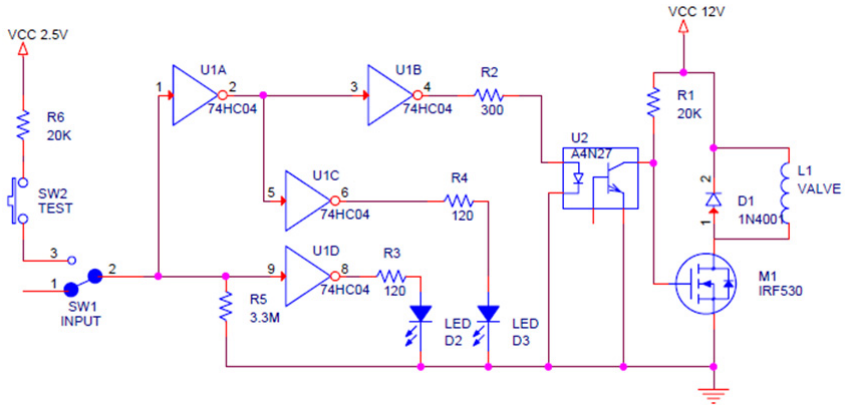

Figure 52 Valve control circuit

When circurecive positive input signal (2.5V) It travels to series of inverters U1A and U1B to optic switch U2 this optic switch component controls transistor M1 that sends current to valve L1.

Experimental testing of the sorting system showed a significant variation in bead arrival times due to wide range of velocities of individual beads in the capillary (Figure 53 Distribution of bead arrival times in 100mkmID capillary at pressure 6atm (075P2NO12 and INKX051185A valve).).

There are several factors causing velocity spread. First of all, because of boundary conditions for the flow in the capillary, velocity if the fluid in laminar regime has parabolic dependence within the range 0<V<Vmax, where Vmax=2V average. Secondly, since our beads

have significant diameter (5mkm) compared to the capillary ID (50 -100mkm), distribution of the beads over the capillary cross-section depends on the volumetric speed of the flow in the capillary. Another reason for variation of beads' velocity is disturbance of the capillary flow introduced by working valve.

Fig. 53 was measured using the sorting system described above. We measured fraction of the sorted beads depending on the delay time set between detection and valve opening (arrival time). In order to measure the bead arrival time we put the valve hold equal to 50ms, and increased the delay time between the detector and the valve from 1ms to 250ms. As can be seen, the bead arrival time varies by about order of magnitude.

As can be seen from Figure 53 Distribution of bead arrival times in 100mkmID capillary at pressure 6atm (075P2NO12 and INKX051185A valve)., left, fraction of sorted beads reached its maximum for 50ms delay time. Based on the performed measurements we found that velocities of the beads are distributed between 0.1 and 1.5m/s for 7 atm. applied pumping pressure.

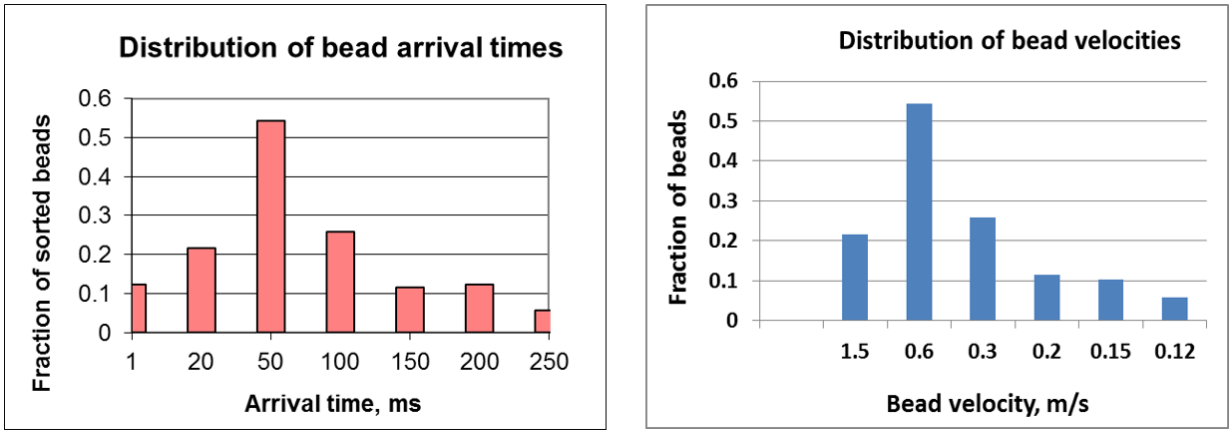

Figure 53 Distribution of bead arrival times in 100mkmID capillary at pressure 6atm (075P2NO12 and INKX051185A valve).

Because of that, that was impossible to determine accurately the delay time between bead detection and bead sorting events. Therefore, in order to collect all CNV-positive beads we had to increase the valve hold time up to 250ms, which is much longer than the time needed for the valve switching.

Uncertainty in the bead arrival time to the sorting spot lead to either large (up to 90%) loss of CNV-beads (in case of small valve hold time) or very low enrichment efficiency (E=56%) in case of the long hold time, when many non-CNV beads were directed to the sort vial.

Obviously, delay times and their variations are proportional to **L**. Therefore if we would like to improve parameters of the system, we need to shorten L.

In our system, due to the use of capillary/tubing connectors, the distance **L** between the bead detection spot and sorting spot in T-junction is ~70mm.

It's important to emphasize that our system requirements are such that the distance between two consecutive beats must be larger than diameter of the laser beam (~100mkm). It means, that if we want to sort out 1% of useful beads, the distance between the useful beads will be ~20mm (taking into account poisson distribution in beads' arrival). Therefore, in the first design with L= 70mm we have simultaneously several useful beads within L distance. In this case velocities of consecutive beads depend on valve switching. This factor would introduce additional uncertainty in the arrival time of the beads.

In order to improve the system's performance I designed a second system with reduced distance L (L=17mm).

4.4.Second system design

In second system design I used direct integration of a silica capillary into silicone tubing. This type of connection reduced distance from registration point to sorting point almost three times from 50mm to 17mm. Also we significantly reduced the inner volume of the tubing.

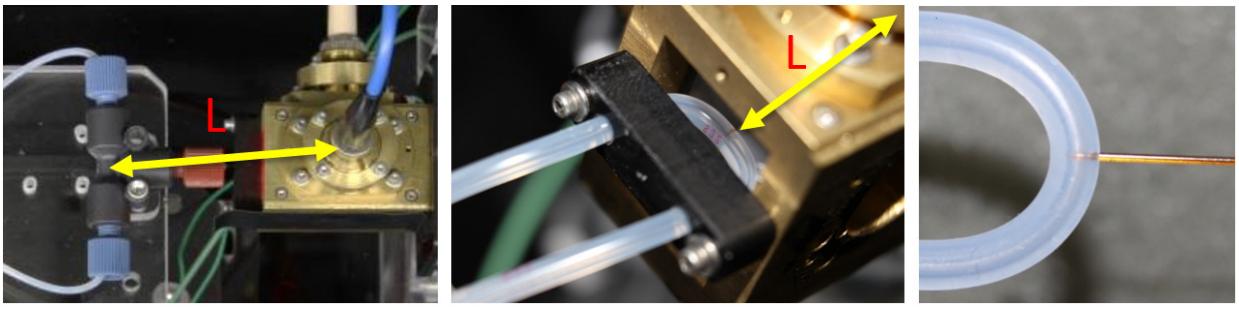

Figure 54. Second system design

As can be seen, in order to further reduce distance L one needs to change the design of the optical head. This is a very big challenge since optical head is highly optimized for light illumination/collection efficiency, easiness and reproducibility of manipulations with the capillary, robustness, and cost. Thus, L=17mm is a minimum length we could achieve in the capillary sorter. Further reduction of L is only possible using micro-fluidic chip.

4.5.Measurement of bead velocity

The problem of the sorting system is that beads in the capillary move at different velocities $\mathbf{V_{BEAD}}$. As a result, time needed for the bead to move from the **detection spot** to the **T-junction** (distance **L** on the Figure 1A) varies from bead to bead. **To solve the problem, we need to calculate individual delay times $\mathbf{d1_{BEAD}}$ for every bead:**

$$\mathbf{d1_{BEAD} = V_{BEAD} / L}$$ where $\mathbf{V_{BEAD}}$ is velocity of the bead.

In order to find $\mathbf{V_{BEAD}}$ we will use the **time width** of the fluorescent peak which is detected when the bead crosses the laser beam at the detection spot **(**see Figure 55 Laser beam of diameter D in the capillary: schematic (left panel) and view A (photo) (right panel).) below, which shows a capillary illuminated with laser beam and a bead which moves in the capillary).

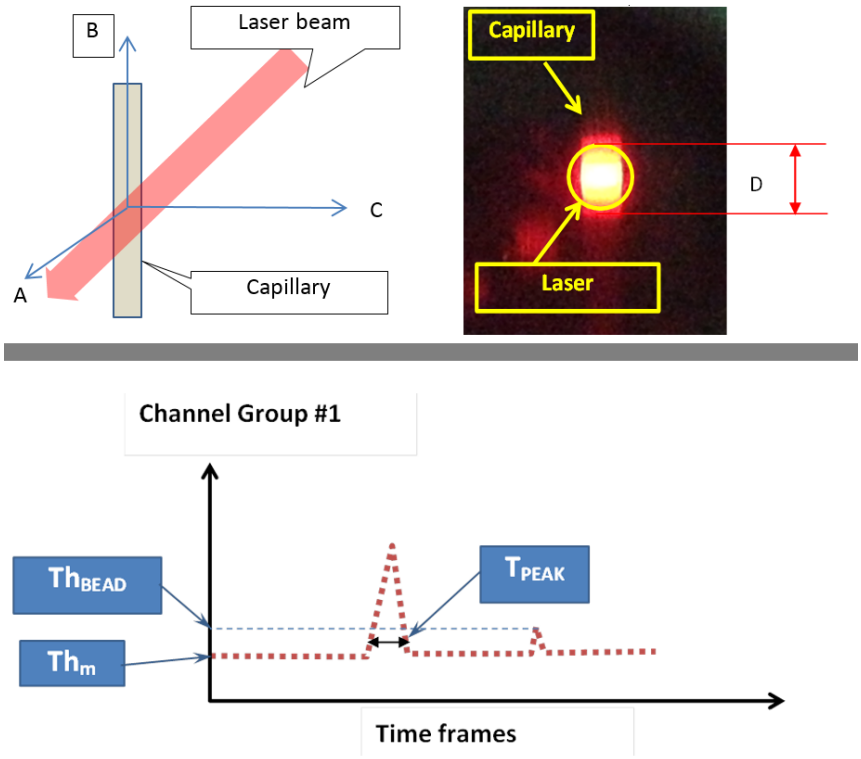

Figure 55 Laser beam of diameter D in the capillary: schematic (left panel) and view A (photo) (right panel).

For accurate measurements of the velocity of the bead we align optical head so that diameter D ic larger than capillary ID (D-80um and ID-50um).

When the bead crosses the laser beam (see **View A**) it produces a fluorescence peak of duration $\mathbf{T_{PEAK}}$. The peak is detected by PMT and counted by FPGA. In this case

$$V_{BEAD} = {}^{D}/_{T_{PEAK}} \quad \text{and} \quad d1_{BEAD} = {}^{L \times T_{PEAK}}/_{D}$$

When the laser beam excites fluorescence of the bead, the detected photon count is processed by the FPGA counter. In case if ratio **R** satisfies certain criteria, FPGA sends a control signal to the valve which opens the sorting channel for a short time for collection of the sorted bead.

In order to minimize the valve open time and since there is a distance **L** between the spot where the bead is detected and the **T-junction** where the bead is sorted, **the control signal from the FPGA to the valve may be delayed.** The delay time must be chosen such that by the time when the bead reaches the **T-junction**, the valve is already opened.

$$E = \frac{N_{SORT}}{N_{TOTAL}} = \frac{\sum n_{SORT} \times \tau_{SORT}}{T_{TOTAL}}$$

$$\tau_{SORT} = \tau_{DELAY} + \tau_{VALVE\ HOLD\ TIME} + \tau_{VALVE\ OPEN/CLOSE\ TIME}$$

Figure 56 shows distribution of bead velocities for two pumping pressures and depending on operation of the valve

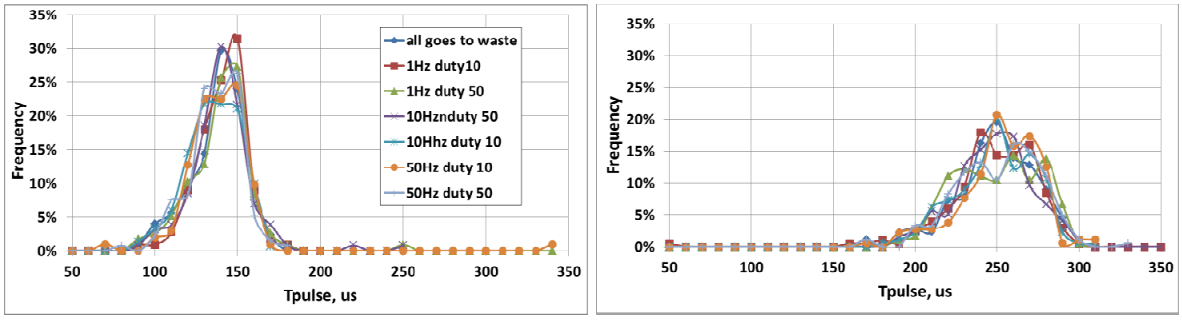

Figure 56 Laser beam of diameter D in the capillary: schematic (left panel) and view A (photo) (right panel).

As can be seen, operation of the valve disturb the peak time for ~10-15%.

Figures 57-58 present block diagram and photographs of the setup for checking the proposed method of bead velocity measurements.

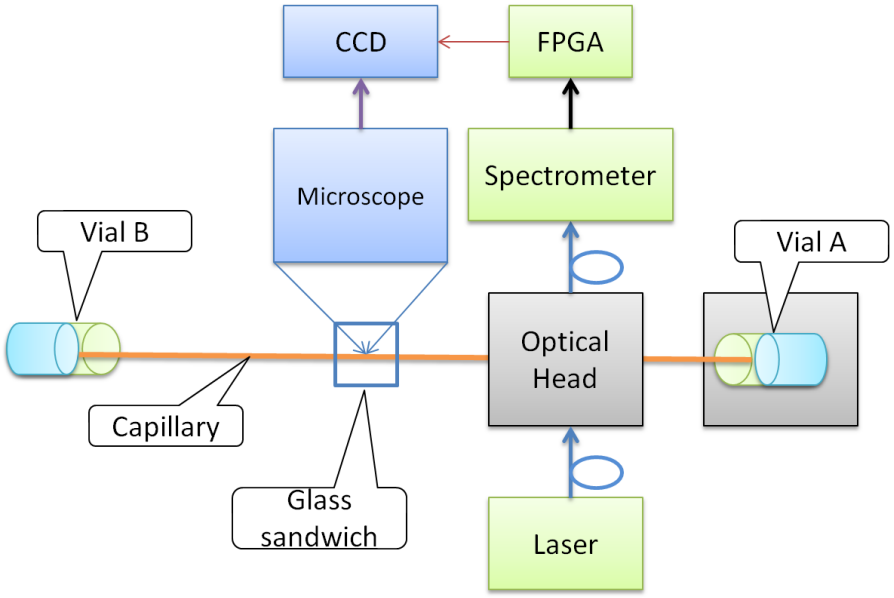

Figure 57. Block diagram for measurements of bead velocities, simulation of the valve operation, and control of adaptive delay time sorting method.

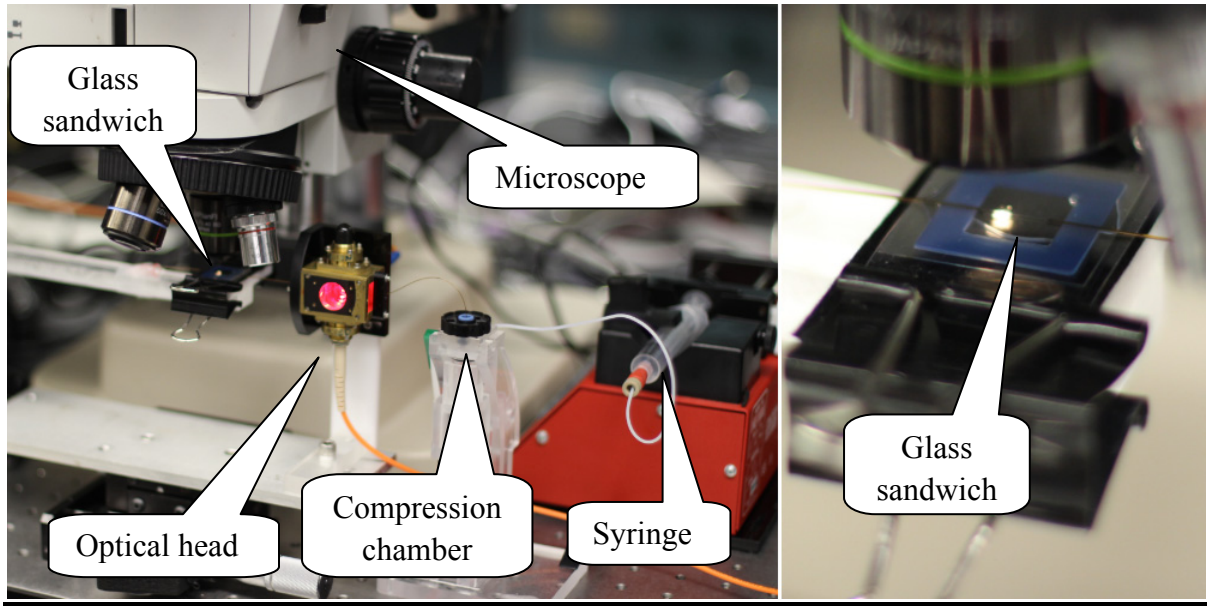

Figure 58. Experimental setup for measurements of bead velocities, simulation of the valve operation, and control of adaptive delay time sorting method.

The main goal of this system is to check whether or not mechanical sorting destroys conditions for adaptive delay technique.

In this setup, beads are injected into the capillary using air pumping. After detection in the optical head by the photon detector, the beads are pushed through the capillary, which is installed on the microscope. The photon detector triggers CCD or CMOS camera, which records images of the beads in the capillary. By using this method one can control velocities of individual beads, position of the beads in the capillary, and check accuracy of the method for generation of the adaptive delay time, as well as measure distribution of the beads' velocity.

Advantages:

- No bead loss
- Multiple sorting objects:
  - Beads
  - Cells
  - Emulsion droplets
- Detection speed up to 10^5/s

- Sorting speed up to 10^4/s
- Small size and low cost

Innovation

The major innovation of this work is a novel approach to fluorescence activated sorting of low abundant micro-objects. Due to a significant difference in the detection and sorting speeds, one can use a cycling enrichment for very high speed, high accuracy sorting of micro-objects such as beads, cells and others. The predicted technical and economic performance of the sorting system exceeds commercial FACS systems.

Significance

The proposed method for detection and identification of CNVs at whole-genome level reduces cost per patient by almost 10 fold. This is an enabling factor for population wide studies of CNVs, which will not only help do discover disease associated CNVs, but also will reveal influence of various environmental factors on genetic alterations.

The proposed system for fluorescence activated enrichment and sorting of CNVs has universal character. Indeed, our approach to the sorting can be implemented both on chip and using mini-fluidics (micro-tubing, capillaries, etc.). The sorting speed of the system is comparable to existing FACS machines. Simultaneously, the loss of particles in the system is ~10 folds less than in commercial FACS systems.

Due to universal character of the sorter, this instrument can also be used for sorting circulating tumor cells, isolation of individual cells for single cell studies and other applications based on fluorescence activated sorting.

4.6.Future work

Development of the automated capillary bead sorter and chip-based bead sorter.

The chip topology allows:

Generation of water-oil droplets for emulsion PCR on beads using inlet 1 for the sample and inlets 2 for oil; 3-way sorting using outlets 3 and 4 for non-CNV beads and the beads with two different CNV ratios respectively

Development of chip-based fluorescence activated bead sorter

We have completed the design of the confocal optical system for chip-based fluorescence activated bead sorter Figure 59. layout of the optical system and CAD simulation and optimization of the system performance.

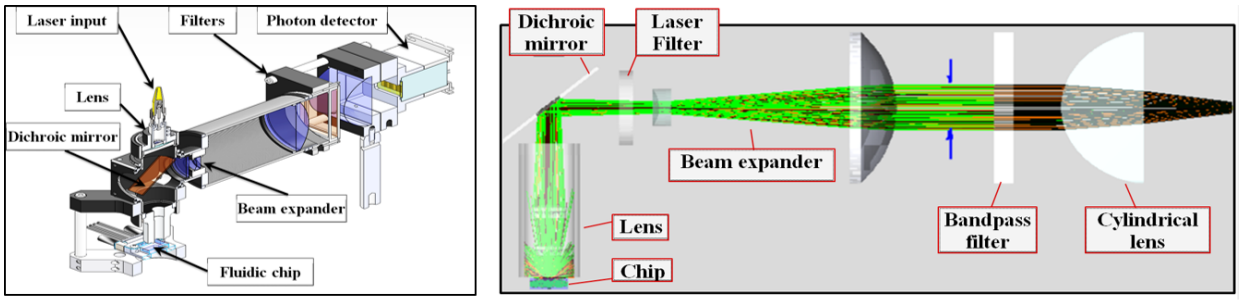

Figure 59. layout of the optical system and CAD simulation and optimization of the system performance.

In the system, the laser beam passes through the beam shaper, dichroic beam splitter, and gets focused onto the micro-channel of the fluidic chip by the objective. Due to the use of the beam shaper, the illuminated zone of the channel has an optimum geometry (120um x 20um), which provides uniform illumination of the channel. When individual beads pass through the illuminated zone, the excited fluorescence is collected by the same lens, passes through a beam shaper/expander and appropriate band-pass filters, and is impinged onto the photon detector (PMT H-7260, Hamamatsu). We have already completed optical simulations of the system and have determined a set of optimum commercial components (see Commercialization Plan for detailed system design). The simulation results showed that in optimum configuration the system can provide ~ 1% fluorescence collection efficiency

Development of a concept for automated capillary fluorescence activated bead sorter

Simultaneously, we have carried out computer aided design optical system for the chip-based sorter because of its universality (can be used in conjunction with various chip topologies), higher sorting speed, much better fluidic control providing higher sorting accuracy, and more than one sorting output. Figure 60. Automated capillary bead sorter. Schematic (left). General view of the instrument (right)

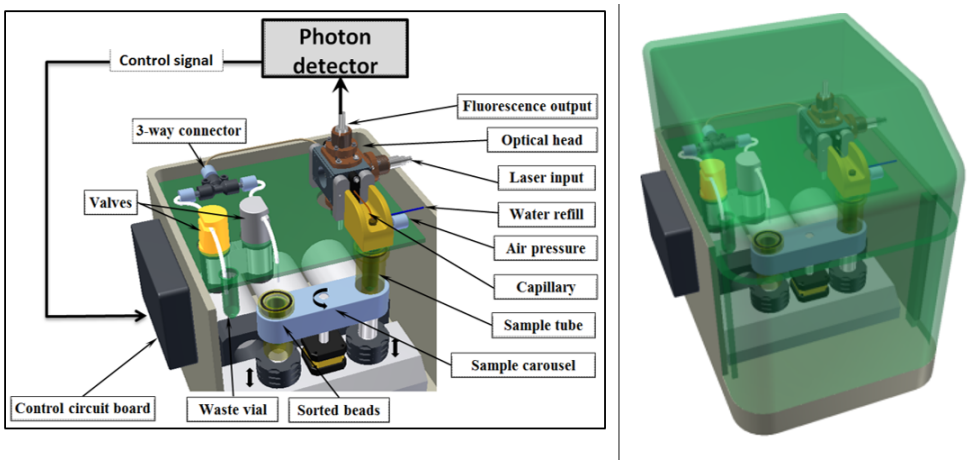

Figure 60. Automated capillary bead sorter. Schematic (left). General view of the instrument (right)

In this instrument the beads from the sample tube go through capillary, get detected in the optical system and sorted in the 3-way connector by an appropriate operation of two valves. The valves obtain the control signal for sorting from the FPGA chip which is built into the photon detector. As soon as the sorting cycle is finished, the FPGA chip makes calculation of the sample enrichment, and if the enrichment is below the required, the sample carousel brings the sorted vial to the original position of the sample tube, the vial gets refilled with water and sorting cycle is repeated.

II. CONCLUSION

I have developed a universal data acquisition system for measurements of multi-color fluorescence in Life Science applications. The system fully satisfies the goal which has been set in the beginning of my work: Development of universal data acquisition system for ultra-sensitive and highly accurate detection of very weak fluorescent signals from biological objects.

Unique features of the developed system include:

- Supports wide variety of tests and chemistries

- Most detailed and accurate measurement of fluorescent signals enabling any desired data processing
- Single photon sensitivity
- Low reagent consumption (*low dead volume*)
- Ability of repetitive runs of the same samples in different conditions
- No equipment conservation needed
- Ease of use and maintenance
- Modular (plug & play) architecture

Application of the system in three most widely used areas have been demonstrated and tested:

- Multi-color fluorometry
- Detection and recognition of color-encoded beads
- DNA sequencing by capillary electrophoresis

We believe that due to an extremely high sensitivity of the photon detection in conjunction with method for highly accurate color decomposition, the developed system may be very useful for detection and decoding of multiple color codes and it can be used in various applications which require highly accurate identification of biological samples labeled with multiple fluorescent colors.

III. BIBLIOGRAPHY

Alaverdian L., Alaverdian S., Bilenko O., Bogdanov I., Filippova E., Gavrilov D., Gorbovitski, B. Gouzman, M. Gudkov G., Domratchev S., Kosobokova O., Lifshitz N., Luryi S., Ruskovoloshin V., Stepukhovich A., Tcherevishnick M., Tyshko G., Gorfinkel V., "A family of novel DNA sequencing instruments based on single photon detection" Electrophoresis 23, pp. 2804-2817, 2002.

Braeckmans, K.; de Smedt, S.; Roelant, C.; Leblans, M.; Pauwels, R.; Demeester, J. Nat., "Encoding microcarriers by spatial selective photobleaching," Mater. (2003), 2, 169-193.

Gao, X.; Nie, S., „Doping Mesoporous Materials with Multicolor Quantum Dots" *J. Phys. Chem. B*, 2003, *107* (42), pp 11575–11578

Gao X., Nie S., "QD-encoded mesoporous beads with high brightness and uniformity: rapid readout by flow cytometry" Analytical Chemistry 2004,76, 2406-2410.

Grondahl, L.; Battersby, B. J.; Bryant, D.; Trau, M. "Encoding Combinatorial Libraries: A Novel. Application of Fluorescent Silica Colloids," Langmuir 2000, 16, 9709-9715.

Gudkov D., Gavrilov D., Tsupryk A., Tovkach I., Gudkov G., Kosobokova O., Cherevishnik M. Gorbovitski B.*), Gorfinkel V., "Detection of multi-color fluorescent objects with single photon detector", 2012, accepted for publication in Biosensors and Bioelectronics.

Dejneka, M. J.; Streltsov, A.; Pal, S.; Frutos, A. G.; Powell, C. L.; Yost, K.; Yuen, P. K.; Muller, U.; Lahiri, J. "Rare earth-doped glass microbarcodes," Proc. Natl. Acad. Sci. U.S.A. 2003, 100, 389-393.

Ful, A., Gu, W.; Larabell, C.; Alivisatos, A.P. "Semiconductor nanocrystals for biological imaging"; Current Opinion in Neurobiology 2005, 15:568–575

Mulvaney, S. P.; Musick, M. D.; Keating, C. D.; Natan, M. J., "Glass-coated, analyte-tagged nanoparticles: A new tagging system based on detection with surface-enhanced Raman scattering," Langmuir 2003, 19, 4784-4790.

Nicewarner-Pena, S. R.; Freeman, R. G.; Reiss, B. D.; He, L.; Pena, D. J.; Walton, I. D.; Cromer, R.; Keating, C. D.; Natan, M. J. "Submicrometer metallic barcodes," Science 2001, 294, 137-141.

Tsupryk A., Tovkach I., Gavrilov D., Kosobokova O., Gudkov G., Tyshko G., Gorbovitski B., and Gorfinkel V., "Ultra sensitive sensor with enhanced dynamic range for high speed detection of multi-color fluorescence radiation," Biosensors and Bioelectronics Volume: 23, Issue: 10, Pages: 1512-1518.

A. Wolff, I. R. Perch-Nielsen, U. D. Larsen, P. Friis, G. Goranovic, C. R. Poulsen, J. P. Kuttera and P. Tellemana "Integrating advanced functionality in a microfabricated high-throughput fluorescent-activated cell sorter"

Dino Di Carlo "Inertial microfluidics" published as an Advance Article on the web 22nd September 2009

Daniel R. Gossett &Westbrook M. Weaver & Albert J. Mach & Soojung Claire Hur & Henry Tat Kwong Tse &Wonhee Lee & Hamed Amini & Dino Di Carlo "Label-free cell separation and sorting in microfluidic systems" Anal Bioanal Chem (2010)